Supporting Information: Three States Involving Vibronic Resonance Is a Key to Enhancing Reverse Intersystem Crossing Dynamics of an Organoboron-Based Ultrapure Blue Emitter

Inkoo Kim,[†] Kwang Hyun Cho,[‡] Soon Ok Jeon,[¶] Won-Joon Son,[*,†] Dongwook Kim,[*,§] Young Min Rhee,[*,‡] Inkook Jang,[†] Hyeonho Choi,[¶] and Dae Sin Kim[†]

[†]*Data and Information Technology Center, Samsung Electronics, Hwaseong 18448, Republic of Korea.*

[‡]*Department of Chemistry, Korea Advanced Institute of Science and Technology (KAIST), Daejeon 34141, Republic of Korea.*

[¶]*Samsung Advanced Institute of Technology, Samsung Electronics, Suwon 16678, Republic of Korea.*

[§]*Department of Chemistry, Kyonggi University, Suwon 16227, Republic of Korea.*

E-mail: wonjoon.son@samsung.com; dongwook-kim@kyonggi.ac.kr; ymrhee@kaist.ac.kr

Supporting Information Texts

1. Spin–vibronic model

Details of the centerpiece of our spin–vibronic model for RISC have been described elsewhere.[S1] In essence, the electronic wavefunctions of the S_1–T_1 spin–orbit coupling element, $\langle S_1, \nu' | \hat{H}_{SO} | T_1, \nu \rangle$, are first perturbatively expanded in the singlet and the triplet manifolds to reflect the non-Born–Oppenheimer vibronic coupling, and then the coupling element within the spin–vibronic model is obtained by collecting the second-order terms that possess both the spin–orbit (SO) and the non-Born–Oppenheimer (nBO) terms. These are brought into the golden rule formula in combination with the first-order direct spin–orbit (DSO) coupling term. We assumed that DSO coupling between a pair of any singlet and triplet states is constant (Condon approximation). While we considered only the expansion in the triplet spin-manifold in ref S1, we extended the spin–vibronic model here to further incorporate the singlet manifold for a more complete and quantitative treatment of the second-order contribution to k_{RISC}.

With the Condon approximation, the vibronic integrals of DSO coupling can be written as

$$\langle S_J, \nu' | \hat{H}_{SO} | T_I^M, \nu \rangle \simeq \langle S_J | \hat{H}_{SO} | T_I^M \rangle \, \langle \nu' | \nu \rangle \tag{S1}$$

where I and J label excited states while ν and ν' denote vibrational states. Of course, M represents the projected spin quantum number. The electronic spin–orbit coupling in the right-hand-side of this equation can be effectively described with the one-electron Breit–Pauli Hamiltonian (see e.g., ref S2).

To the first order, the nBO coupling between two vibronic states of the same spin sym-

metry can be approximated as[S3]

$$\langle \mathrm{X}_J, \nu' | \hat{H}_{\mathrm{nBO}} | \mathrm{X}_I, \nu \rangle \simeq \sum_{\kappa} \langle \mathrm{X}_J | \hat{P}_\kappa | \mathrm{X}_I \rangle \langle \nu' | \hat{P}_\kappa | \nu \rangle \tag{S2}$$

with $\mathrm{X} = \mathrm{S}, \mathrm{T}$. Here, $\hat{P}_\kappa \equiv -\mathrm{i}\hbar\, \partial/\partial Q_\kappa$ is the momentum operator in the κth normal coordinate Q_κ. The electronic part of the derivative coupling between the excited states can be efficiently calculated, for instance, with TDDFT.[S4]

Substituting eqs S1 and S2 with $\langle \nu' | \nu'' \rangle = \delta_{\nu',\nu''}$, the coupling (eq 1 in the main text) can then be cast into

$$H'_M = \langle \mathrm{S}_1 | \hat{H}_{\mathrm{SO}} | \mathrm{T}_1^M \rangle \langle \nu' | \nu \rangle + \sum_{\kappa} (t_\kappa^M + s_\kappa^M) \langle \nu' | \hat{P}_\kappa | \nu \rangle \tag{S3}$$

with

$$t_\kappa = \frac{1}{2} \sum_{n=2} \langle \mathrm{S}_1 | \hat{H}_{\mathrm{SO}} | \mathrm{T}_n \rangle \langle \mathrm{T}_n | \hat{P}_\kappa | \mathrm{T}_1 \rangle \left(\frac{1}{E_{\mathrm{T}_n} - E_{\mathrm{T}_1}} + \frac{1}{E_{\mathrm{T}_n} - E_{\mathrm{S}_1}} \right) \tag{S4}$$

$$s_\kappa = \frac{1}{2} \sum_{n=2} \langle \mathrm{S}_1 | \hat{P}_\kappa | \mathrm{S}_n \rangle \langle \mathrm{S}_n | \hat{H}_{\mathrm{SO}} | \mathrm{T}_1 \rangle \left(\frac{1}{E_{\mathrm{S}_n} - E_{\mathrm{T}_1}} + \frac{1}{E_{\mathrm{S}_n} - E_{\mathrm{S}_1}} \right) \tag{S5}$$

which represent the second-order contributions from the triplet and the singlet manifolds, respectively. We note that a semi-classical approximation has been employed to remove vibrational energy dependencies in the denominators. Figure 3b in the main text was obtained by treating the contributions by t_κ and s_κ in a separate manner to perform a quantitative analysis of the relative second-order contributions by different spin manifolds with the terms defined in eq 4 in the main text.

Finally, the golden rule rate expression (eq 1 in the main text) can be rewritten as

$$\begin{aligned} k_{\mathrm{RISC}} = & \frac{2\pi}{\hbar} \sum_{\nu\nu'} P_\nu(T) \left[K_{\mathrm{SO}} \langle \nu | \nu' \rangle \langle \nu' | \nu \rangle + \sum_{\kappa\kappa'} (T_{\kappa\kappa'} + S_{\kappa\kappa'} + C_{\kappa\kappa'}) \langle \nu | \hat{P}_\kappa | \nu' \rangle \langle \nu' | \hat{P}_{\kappa'} | \nu \rangle \right] \\ & \times \delta(-\Delta E_{\mathrm{ST}} + E_\nu - E_{\nu'}) \end{aligned} \tag{S6}$$

with the following coupling element and matrices:

$$K_{\mathrm{SO}} = \frac{1}{3}\sum_{M}\left|\langle \mathrm{S}_1|\hat{H}_{\mathrm{SO}}|\mathrm{T}_1^M\rangle\right|^2 \tag{S7}$$

$$\mathbf{T} = \sum_{M}\vec{t}^{M}\vec{t}^{M\dagger} = \frac{1}{3}\Re[\mathbf{T}^{(0)} + 2\mathbf{T}^{(1)}] \tag{S8}$$

$$\mathbf{S} = \sum_{M}\vec{s}^{M}\vec{s}^{M\dagger} = \frac{1}{3}\Re[\mathbf{S}^{(0)} + 2\mathbf{S}^{(1)}] \tag{S9}$$

$$\mathbf{C} = 2\sum_{M}\vec{t}^{M}\vec{s}^{M\dagger} = \frac{2}{3}\Re[\mathbf{C}^{(0)} + 2\mathbf{C}^{(1)}] \tag{S10}$$

where $\vec{t}$ and $\vec{s}$ are the vectors formed by $\{t_\kappa\}$ and $\{s_\kappa\}$. Thermal averaging over the triplet substates are conveniently encoded in the above equations. We note that the time-reversal symmetry has been imposed in the derivation. As a result, the cross-term between the first- and the second-order vanishes, and the second-order coupling becomes real-valued. Previously in ref S1, the contributions by $\mathbf{S}$ and $\mathbf{C}$ were neglected. Under the harmonic approximation, the analytical solution for eq S6 can be obtained in the framework of a correlation function.[S1,S5–S7] This is in conjunction with Duschinsky transformations,[S8] which furnishes a linear relationship between two geometries and the corresponding normal coordinates, $\mathbf{Q}_{\mathrm{T}_1} = \mathbf{Q}_{\mathrm{S}_1}\mathbf{J} + \mathbf{d}$, where $\mathbf{J}$ is the mode-mixing matrix and the vector $\mathbf{d}$ is the displacement between the harmonic vibrational parabolas. By Fourier transforming the δ-function with the scaled time $\tau = t/\hbar$, one can finally arrive at the rate equation in the time domain,

$$\begin{aligned} k_{\mathrm{RISC}} = &\frac{1}{\hbar Z}\int_{-\infty}^{\infty}\mathrm{d}\tau\ \exp(-\mathrm{i}\Delta E_{\mathrm{ST}}\tau)\rho_{\mathrm{DSO}}(\tau,\tau') \\ &\times\left(K_{\mathrm{SO}} + \sum_{\kappa\kappa'}(T_{\kappa\kappa'} + S_{\kappa\kappa'} + C_{\kappa\kappa'})\chi_{\mathrm{SV}}(\tau,\tau';\kappa,\kappa')\right) \end{aligned} \tag{S11}$$

and the correlation functions $\rho_{\mathrm{DSO}}(\tau,\tau')$ and $\chi_{\mathrm{SV}}(\tau,\tau';\kappa,\kappa')$ bear analytical solutions from

the path-integral formulation:[S1]

$$\rho_{\mathrm{DSO}}(\tau,\tau') = \sqrt{\frac{\mathrm{prod}(\mathbf{a})\,\mathrm{prod}(\mathbf{a}')}{\det(\mathbf{K})}}\exp\left(-\frac{\mathrm{i}}{\hbar}\left[\frac{1}{2}\mathbf{f}^T\mathbf{K}^{-1}\mathbf{f} - \mathbf{d}^T\mathbf{E}\mathbf{d}\right]\right) \tag{S12}$$

$$\chi_{\mathrm{SV}}(\tau,\tau';\kappa,\kappa') = \mathrm{i}\hbar\,\mathrm{Tr}[\mathbf{G}(\kappa,\kappa')\mathbf{K}^{-1}] + [\mathbf{K}^{-1}\mathbf{f}]^T\mathbf{G}(\kappa,\kappa')[\mathbf{K}^{-1}\mathbf{f}] - \mathbf{h}^T(\kappa,\kappa')[\mathbf{K}^{-1}\mathbf{f}] \tag{S13}$$

where $\tau' = -\tau - \mathrm{i}(k_{\mathrm{B}}T)^{-1}$ and the intermediate matrices and vectors are defined by

$$\mathbf{E} = \mathrm{diag}(\mathbf{b}' - \mathbf{a}') \tag{S14}$$

$$\mathbf{K} = \begin{bmatrix} \mathbf{B} & -\mathbf{A} \\ -\mathbf{A} & \mathbf{B} \end{bmatrix} \tag{S15}$$

$$\mathbf{A} = \mathrm{diag}(\mathbf{a}) + \mathbf{J}^T\,\mathrm{diag}(\mathbf{a}')\mathbf{J} \tag{S16}$$

$$\mathbf{B} = \mathrm{diag}(\mathbf{b}) + \mathbf{J}^T\,\mathrm{diag}(\mathbf{b}')\mathbf{J} \tag{S17}$$

$$\mathbf{f} = \begin{bmatrix} \mathbf{d}^T\mathbf{E}\mathbf{J} & \mathbf{d}^T\mathbf{E}\mathbf{J} \end{bmatrix}^T \tag{S18}$$

$$\mathbf{G}(\kappa,\kappa') = \begin{bmatrix} \mathbf{G}_{11}(\kappa,\kappa') & \mathbf{G}_{12}(\kappa,\kappa') \\ \mathbf{G}_{21}(\kappa,\kappa') & \mathbf{G}_{22}(\kappa,\kappa') \end{bmatrix} \tag{S19}$$

$$\mathbf{h}^T(\kappa,\kappa') = \begin{bmatrix} \mathbf{h}_1^T(\kappa,\kappa') & \mathbf{h}_2^T(\kappa,\kappa') \end{bmatrix} \tag{S20}$$

with their elements given as

$$a_\mu = \omega_\mu / \sin(\hbar\omega_\mu\tau) \tag{S21}$$

$$b_\mu = \omega_\mu / \tan(\hbar\omega_\mu\tau) \tag{S22}$$

$$a'_\mu = \omega'_\mu / \sin(\hbar\omega'_\mu\tau') \tag{S23}$$

$$b'_\mu = \omega'_\mu / \tan(\hbar\omega'_\mu\tau') \tag{S24}$$

$$G_{11,\mu\nu}(\kappa,\kappa') = -\delta_{\mu\kappa'}b'_\kappa[\mathbf{J}^T\,\mathrm{diag}(\mathbf{a}')\mathbf{J}]_{\kappa\nu} \tag{S25}$$

$$G_{12,\mu\nu}(\kappa,\kappa') = \delta_{\mu\kappa'}b'_\kappa[\mathbf{J}^T\,\mathrm{diag}(\mathbf{b}')\mathbf{J}]_{\kappa\nu} \tag{S26}$$

$$G_{21,\mu\nu}(\kappa,\kappa') = \delta_{\mu\kappa'}a'_\kappa[\mathbf{J}^T\,\mathrm{diag}(\mathbf{a}')\mathbf{J}]_{\kappa\nu} \tag{S27}$$

$$G_{22,\mu\nu}(\kappa,\kappa') = -\delta_{\mu\kappa'}a'_\kappa[\mathbf{J}^T\,\mathrm{diag}(\mathbf{b}')\mathbf{J}]_{\kappa\nu} \tag{S28}$$

$$h_{1,\mu}(\kappa,\kappa') = \delta_{\mu\kappa'} b'_{\kappa} [\mathbf{d}^T \mathbf{E} \mathbf{J}]_{\kappa} \tag{S29}$$

$$h_{2,\mu}(\kappa,\kappa') = -\delta_{\mu\kappa'} a'_{\kappa} [\mathbf{d}^T \mathbf{E} \mathbf{J}]_{\kappa} \tag{S30}$$

In practice, we found the time integration interval of [−6553.6:6553.6] fs with a time step of 0.1 fs to be satisfactory from the viewpoint of both cost and precision, and hence we used these conditions for calculating all correlation functions here. Also with the adopted conditions, the time correlation functions well converged to zero and stayed there in the long time limit (for instance, Figures S11 and S12).

2. Quantum chemical calculations

As discussed in the main text, accurately predicting the relative energies as well as the geometries of the involved excited states is of the key importance for elucidating any excited-state dynamics. We employed the SCS-ADC(2)/SVP level of theory for geometry optimizations as it can incorporate higher-order electron correlation effects into the excited states. The optimized geometries and the corresponding vibrational frequencies with the scaling factor 0.9631 as suggested in ref S9 are provided in Tables S5 and S6. At these geometries, the excited state energy gaps with various levels of theory were additionally calculated to assess the performance of the methods (Table S3). In comparison with the experimental data in the solution phase, ΔE_{ST} from the SCS-CC2 level agrees quite well, while SCS-ADC(2) slightly underestimates the energy gap. A number of progressively larger basis sets were also tested to evaluate the basis set effect on ΔE_{ST}. From this, we only observed slight shifts. We note that even the gap-tuned DFT functional ω^*B97X substantially overestimates the singlet–triplet gap, mostly due to the lack of higher-order correlations. However, due to the unavailability of the spin–orbit coupling and the derivative coupling between excited states in both CC2 and ADC(2) methods, we have resorted to the gap-tuned ω^*B97X for computing those elements. At least, we attested for a reproduction of the triplet–triplet gap ΔE_{TT}, which can dominate the magnitude of the nonadiabatic coupling. As is common

with molecules containing only light elements, scalar relativistic effect was not considered. The electronic structure of the excited states were compared with the ADC(2) results using the natural transition orbital (NTO) analysis to match the ordering of excited states. For readers who are curious about the transition characters, we have also listed the hole–particle NTO pairs related to the 18 each lowest singlet and triplet excited states in Figure S4.

3. Well-defined character of $k_{\mathbf{RISC}}$

The Fermi golden rule rate expressions given by eq S6 and by eq 1 in the main text possess a δ-function, which will contribute infinitely whenever the discrete vibrational distribution function P_ν overlaps with the infinity condition of the δ-function. This potential divergence issue arises because eq S32 is constructed without considering any dephasing or broadening effects that do exist in nature, and can be avoided by introducing some damping through replacing the δ-function with a sharp Lorentzian or Gaussian function with a damping time γ.[S10,S11] For example, the Lorentzian function will take the form of

$$\delta'(-\Delta E_{\mathrm{ST}} + E_v - E_{v'}) = \frac{1}{\pi}\frac{\Gamma}{\Gamma^2 + (\Delta E_{\mathrm{ST}} - E_v + E_{v'})^2} \tag{S31}$$

with $\Gamma = h/\gamma$. Often, γ cannot be known with accuracy, and there may be situations where the rate calculation leads to some ambiguity. Fortunately for DABNA, this did not happen. Indeed, as shown in Table S9 and Figure S13 the rates were almost identical regardless of the value of γ. Thus, we have chosen the rate obtained at the longest γ value (100 ns) in our discussion in the main text, assuming that the dephasing related to RISC will take a rather long time. In fact, the rate has essentially converged beyond 1 ns, and the value at $\gamma = 100$ ns is practially the same as the rate obtained without any damping.

With this, one may wonder why the rate without any damping does not diverge even with the true δ-function with a potential infinity condition. This convergence can be explained in

the following manner. When the equation is changed into a Fourier transform format:

$$k_{\mathrm{RISC}} = \frac{1}{Z}\int_{-\infty}^{\infty} \mathrm{d}\tau \exp(-\mathrm{i}\Delta E_{\mathrm{ST}})\bar{\rho}(\tau,\tau') \tag{S32}$$

with the total time correlation $\bar{\rho}$ bearing ρ_{DSO} and χ_{SV}, that infinity must get into $\bar{\rho}$ such that it is not bounded in time. Namely, $\bar{\rho}$ will not decay to zero within $\tau = \pm\infty$. This indeed is a valid concern, and the problem can arise because eq S32 is constructed without considering any dephasing or broadening effects that do exist in nature. Namely, both P_ν and δ in eq S6 are discrete and they either overlap to form an infinity or do not overlap to form zero. To see how this diverging condition takes place and then how the problem practically goes away, let us start with the construction of ρ_{DSO}:[S1]

$$\begin{aligned}\rho_{\mathrm{DSO}} =& \sqrt{\frac{\prod_\mu \frac{\omega_\mu}{\sin\omega_\mu t}\prod_\mu \frac{\omega'_\mu}{\sin\omega'_\mu t'}}{\det\begin{pmatrix}\mathbf{B} & -\mathbf{A}\\ -\mathbf{A} & \mathbf{B}\end{pmatrix}}}\exp\left[-\frac{\mathrm{i}}{\hbar}\left(\frac{1}{2}\mathbf{f}^T\mathbf{K}^{-1}\mathbf{f}-\mathbf{d}^T\mathbf{E}\mathbf{d}\right)\right]\\ \equiv& \sqrt{X}\exp\left[-\frac{\mathrm{i}}{\hbar}\left(\frac{1}{2}\mathbf{f}^T\mathbf{K}^{-1}\mathbf{f}-\mathbf{d}^T\mathbf{E}\mathbf{d}\right)\right]\end{aligned} \tag{S33}$$

If we take an approximation such that the Duschinsky rotation is an identity ($\mathbf{J} = \mathbf{1}$), $\mathbf{A}$ and $\mathbf{B}$ become diagonal matrices without any mode-mixing, and after a little math, one can easily show that the prefactor X in the square root of eq S33 becomes

$$\begin{aligned}X =& \frac{\prod_\mu \frac{\omega_\mu}{\sin\omega_\mu t}\prod_\mu \frac{\omega'_\mu}{\sin\omega'_\mu t'}}{\prod_\mu\left[\left(\frac{\omega_\mu}{\tan\omega_\mu t}+\frac{\omega'_\mu}{\tan\omega'_\mu t'}\right)^2-\left(\frac{\omega_\mu}{\sin\omega_\mu t}+\frac{\omega'_\mu}{\sin\omega'_\mu t'}\right)^2\right]}\\ =& \prod_\mu \frac{1}{2\left(\cos\omega_\mu t\cos\omega'_\mu t'-1\right)-\left(\frac{\omega_\mu}{\omega'_\mu}+\frac{\omega'_\mu}{\omega_\mu}\right)\sin\omega_\mu t\sin\omega'_\mu t'} \equiv \prod_\mu X_\mu\end{aligned} \tag{S34}$$

When the pair of vibrational frequencies of the two involved electronic states are close enough as in DABNA, the μ-th component becomes

$$X_\mu = \frac{1}{2}\frac{1}{\cos\left(\omega_\mu t + \omega'_\mu t'\right) - 1} \tag{S35}$$

Substituting $t' = -t - \mathrm{i}\beta\hbar$ and then scaling by a constant such that $\bar{X}_\mu(t=0) = 1$, we have

$$\bar{X}_\mu = \frac{\cosh\beta\hbar\omega'_\mu - 1}{\cos\left[(\omega_\mu - \omega'_\mu)t - \mathrm{i}\beta\hbar\omega'_\mu\right] - 1} \tag{S36}$$

Its oscillating frequency is related to the frequency change $\omega_\mu \to \omega'_\mu$. This explains the slower envelope oscillations shown in Figure S11. From this equation, we can consider two extreme cases in terms of the temperature. (1) In the low temperature limit ($\beta \to \infty$), because $\cosh\beta\hbar\omega'_\mu \approx \sinh\beta\hbar\omega'_\mu \gg 1$ holds, one can trivially show that

$$\bar{X}_\mu = \frac{1}{\cos(\omega_\mu - \omega'_\mu)t + \mathrm{i}\sin(\omega_\mu - \omega'_\mu)t} \tag{S37}$$

In this case, we can easily anticipate that the oscillation will not decay at all. (2) On the other hand, in the high temperature limit ($\beta \to 0$), $\bar{X}_\mu$ of eq S36 behaves quite differently. In this case, in the vicinity of $t = 0$,

$$\bar{X}_\mu \approx -\frac{\left(\beta\hbar\omega'_\mu\right)^2}{\left[(\omega_\mu - \omega'_\mu)t - \mathrm{i}\beta\hbar\omega'_\mu\right]^2} = -\left[\frac{\epsilon}{(\omega_\mu - \omega'_\mu)^2 t^2 + \epsilon^2}\right]^2 \left[(\omega_\mu - \omega'_\mu)t + \mathrm{i}\epsilon\right]^2 \tag{S38}$$

with $\epsilon = \beta\hbar\omega'_\mu$. We can see that the above expression contains a Lorentzian function with a vanishing width ϵ, namely $\epsilon/[(\omega_\mu - \omega'_\mu)^2 t^2 + \epsilon^2]$. Because the other combining term, $[(\omega_\mu - \omega'_\mu)t + \mathrm{i}\epsilon]^2$, does not particularly diverge at all, the whole $\bar{X}_\mu$ starts from 1 at $t = 0$ and quickly decays to zero as t increases. Of course, when t is too large, the expansion becomes invalid and $\bar{X}_\mu$ will rise back. We will discuss this long-term rising in a later paragraph.

At an intermediate temperature, β will neither be too large nor too small. Then, we can

easily imagine that $\bar{X}_\mu$ will behave somewhere in between the two extreme cases. Namely, the envelope will oscillate with the frequency $\omega_\mu - \omega'_\mu$, and at the same time, decay roughly like a Lorentzian. The decay speed will be related to the temperature with $\beta\hbar\omega'_\mu$. When many $\bar{X}_\mu$ values are multiplied together, the decay from $\bar{X} = 1$ to 0 will be very prominent. In addition, if we further include the mode mixing with non-identity **J** according to eqs S16 and S17, the contributions by all different modes with different frequencies will be added in forming $\bar{X}_\mu$. While it will be non-trivial to show their effects in a simple formula, we can surely anticipate that the added oscillations with different frequencies will suppress the overall oscillations in time. Of course, at $t = 0$, all the functions will be in phase, and the amplitude will be large. This is indeed what we observe in Figure S11.

Because there is no dephasing implemented in our equation, the oscillations will rise back again with an inevitable rephasing behavior in the long term. However, that rephasing time will be related to the least common multiple of all $1/(\omega_\mu - \omega'_\mu)$ values for vibronically participating modes $\{\mu\}$. While $1/\omega_\mu$ is a relatively short time, $1/(\omega_\mu - \omega'_\mu)$ tends to be quite long with small frequency changes in DABNA, and the time determined by the common multiple involving many modes will be even much longer. If we imagine integrating eq S32 really in $(-\infty, \infty)$, it will diverge with the recurring peaks in the time correlation. However, adopting that diverging integral is not physically acceptable, as doing so will be to assume a situation without any dephasing effect. Some dephasing will always happen with real molecules at non-zero temperatures. Therefore, the integration should not be continued any longer than the physically acceptable dephasing time. The only ambiguity will be then the length of dephasing time. To eliminate this ambiguity, we have tested to see how long the time correlation function stays at zero without any rephasing behavior. When $\bar{\rho}$ was calculated up to 419.4 ps without any approximation at every 0.1 fs step, it essentially stayed at zero up to the time limit we have taken (Figure S12). With the approximation of $\mathbf{J} = \mathbf{1}$ (eq S34) together with the data in Table S6, we still observed no rephasing behavior with $\bar{X}$ staying at zero up to 10 μs. In the case of DABNA, the fact that the time correlation

decays to zero earlier than 1 ps and never rises back before 10 μs signifies that as long as the dephasing time is longer than 1 ps and shorter than 10 μs, k_{RISC} will essentially be identical no matter what the actual dephasing time is. Surely, the dephasing time will fall within this wide range that we have tested, and the rate obtained with our integration time limit of $\sim$6.5 ps does not bear any dephasing or damping related uncertainty. This surely resolves the mathematical paradox that we mentioned in this section.

Problems with our scheme can happen when the time correlations do not decay even after a reasonable dephasing time, and the recurrence happens earlier than the decay. This happens especially when the temperature is too low ($\beta \rightarrow \infty$), although the frequency changes and the extent of mode mixing can also govern the situation. When the time correlation lasts beyond the system's dephasing time, the δ-function is often modified into a Gaussian or a Lorentzian function. This remedy, however, may be an ad hoc treatment as knowing the dephasing time accurately may not be a trivial task. Fortunately for DABNA, we did not have to take that path. More numerical tests regarding the dephasing correction can be found elsewhere (ref S10) based on formulations that are very similar to our equations. We also refer readers to a recent detailed account (ref S11) on how the rate is affected by enforced damping, although the rate formulation in that reference is different especially when cumulant expansions are adopted. In any case, we stress again that k_{RISC} was not affected at all unless the dephasing time was assumed to be unphysically short with $\gamma \ll 1$ ps (Table S9), or equivalently, unless the δ-function was distorted into an excessively wide form (Figure S13).

Finally, we note that our mathematical proof of the rate convergence in this section depends on the assumption of $\mathbf{J} = \mathbf{1}$, namely the assumption that the vibrations do not change noticeably between S_1 and T_1. The diagonal dominance of $\mathbf{J}$ shown in Figure S6a directly supports this assumption. In addition, when we re-calculated k_{RISC} displayed in Figure 2a of the main text after assuming $\mathbf{J} = \mathbf{1}$, we observed that the rate values remained without any drastic changes as displayed in Figure S14. Therefore, it is not likely that the

convergence property was affected by the approximation.

4. Semiclassical quantum dynamics simulations

To demonstrate the vibrational resonance behavior in RISC, we employed the non-Hamiltonian version of the Poisson bracket mapping equation (PBME-nH).[S12] In PBME-nH, the density matrix evolution is followed by trajectory simulations governed by the equations of motion of the quantal and the mass-weighted classical phase space variables ($\{(r_i, p_i)\}$ and (R, P) respectively, with i spanning the state space $\mathbf{X} = \{\mathrm{S}_1, \mathrm{T}_1, \mathrm{T}_3\}$):

$$\frac{dr_i}{dt} = \frac{dH_m}{\partial p_i} = \frac{1}{\hbar}\sum_j h^{ij} p_j \tag{S39}$$

$$\frac{dp_i}{dt} = -\frac{\partial H_m}{\partial r_i} = -\frac{1}{\hbar}\sum_j h^{ij} r_j \tag{S40}$$

$$\frac{dR}{dt} = \frac{\partial H_m}{\partial P} = P \tag{S41}$$

$$\frac{dP}{dt} = -\frac{\partial V_b}{\partial R} - \frac{2}{(N+4)\hbar}\sum_{i,j}\frac{\partial h^{ij}}{\partial R}\left(r_i r_j + p_i p_j\right) + \frac{N+4}{4(N+4)}\sum_i \frac{\partial h^{ii}}{\partial R} \tag{S42}$$

Details about how the mapping Hamiltonian H_m is defined can be found in ref S12.

The three state electronic Hamiltonian involving $\mathbf{X}$ was taken as the minimal model:

$$\hat{H}^{\mathrm{el}} = \sum_{i\in\mathbf{X}} |i\rangle\, \epsilon_i \,\langle i| + \sum_{i,\, j\in\mathbf{X}} |i\rangle\, V_{ij}^{\mathrm{SOC}} \,\langle j| \tag{S43}$$

as we observed that they participated most importantly with the golden rule calculations. V_{ij}^{SOC} denotes the spin–orbit coupling as listed in Table S7 with $V_{\mathrm{T_1T_3}}^{\mathrm{SOC}}$ fixed as zero. This is supplemented by the phonon Hamiltonian and the electron–phonon coupling as:

$$\hat{H}^{\mathrm{ph}} = \sum_{i\in\mathbf{X}}\sum_{\xi}\left(\frac{P_\xi^2}{2} + \frac{1}{2}\omega_\xi^2 R_\xi^2\right) \tag{S44}$$

$$\hat{H}^{\mathrm{el-ph}} = \sum_{i\in\mathbf{X}}\sum_{\xi}|i\rangle\, c_{i\xi} R_\xi \,\langle i| + C_{\mathrm{r}} R_{\mathrm{r}}\left(|\mathrm{T}_1\rangle\,\langle \mathrm{T}_3| + |\mathrm{T}_3\rangle\,\langle \mathrm{T}_1|\right) \tag{S45}$$

Here, we have explicitly designated the phonon mode index ξ for both P and R. The phonon modes include the intramolecular normal vibrations of the emitter and the surrounding thermal bath motions,[S13] which couple to the state energies through $c_{i\xi}$. The coupling strengths of the emitter normal vibrations are listed in Table S8 in the form of the reorganization energies ($\lambda_\xi = c_{i\xi}^2/2\omega_\xi$). If the reorganization energies in the table are summed up for the emitter modes, it will become the emitter-specific reorganization energy λ_{em}. The thermal bath surrounding the emitter was modeled by a Debye spectral density, $J(\omega) = 2\lambda_{\mathrm{ph}}\omega\omega_c/(\omega^2+\omega_c^2)$, with $\lambda_{\mathrm{ph}} = 20$ cm^{-1} and $\omega_c = 600$ cm^{-1}.

In this work, we slightly modified the integration scheme for the bath momentum toward reducing the computational cost by increasing the time step with additionally considering its second derivative:

$$\frac{d^2P_\xi}{dt^2} \approx -\frac{2}{(N+4)\hbar}\sum_{i,j}\frac{\partial h^{ij}}{\partial R_\xi}\frac{d}{dt}\left(r_i r_j + p_i p_j\right) \tag{S46}$$

$$= -\frac{2}{(N+4)\hbar}\sum_{i,j}\frac{\partial h^{ij}}{\partial R_\xi}\left(\frac{1}{\hbar}\sum_k\left(h^{ik}p_k r_j + r_\lambda h^{jk}p_k\right)\right) + \frac{2}{(N+4)\hbar}\sum_{i,j}\frac{\partial h^{i,j}}{\partial R_\xi}\left(\frac{1}{\hbar}\sum_k\left(h^{ik}r_k p_j + p_i h^{jk}r_k\right)\right) \tag{S47}$$

As an additional effort to further reduce the computational cost, we applied the focused sampling strategy[S14,S15] by initially sampling the system variables to follow $r_i^2 + p_i^2 = 1$ for $i = \mathrm{T}_1$, with the other states satisfying $r_j = p_j = 0$ with $j = \mathrm{S}_1$ or T_3. The bath was assumed to be initially at a thermal equilibrium at $T = 300$ K, and the classical variables were sampled according to the Wigner distribution:

$$\rho_B(R_\xi, P_\xi) = \frac{1}{\pi\hbar}\tanh\frac{\beta\hbar\omega_\xi}{2}\exp\left(-\frac{\tanh\left(\beta\hbar\omega_\xi/2\right)}{\hbar\omega_\xi}\left(P_\xi^2 + \omega_\xi^2 R_\xi^2\right)\right) \tag{S48}$$

We simulated 5000 PBME-nH trajectories for getting the RISC rate at each given condition. Each trajectory was propagated for 1 ps with an integration time step of 0.1 fs. The con-

tinuous spectral density was implemented using 1000 discrete bath modes with a maximum frequency, $\omega_{\max} = 3000$ cm^{-1}. These discrete bath modes recover 98% of the reorganization energy from the continuum bath, λ_{ph}. Because we did not perform T_3 geometry optimizations, the T_1–T_3 reorganization energy was not known, and we employed the identical vibrational coupling as in the T_1–S_1 pair. Among all the bath modes, we designated that one mode ("R_{r}") can induce geometry-dependent vibronic coupling between T_1 and T_3. Because such coupling grows linearly with the displacement from the equilibrium geometry, we adopted a linear coupling coefficient C_{r}. Thus, this coupling changes with the emitter geometry and intrinsically bears a non-Condon character. The magnitude of C_{r} is dictated by the derivative coupling and the adopted quasi-diabatic scheme.[S16,S17] If we define the quasi-diabatic states as the adiabatic states at the T_1 optimized geometry, the derivative of the diabatic Hamiltonian with respect to the nuclear coordinates is obtained from the derivative coupling.[S18] Then, C_{r} can be easily estimated from the projection of the T_1–T_3 derivative coupling vector $\vec{F}$ onto the normal mode vector of R_{r}:

$$C_{\mathrm{r}} = -\left(E_{\mathrm{T}_3} - E_{\mathrm{T}_1}\right) \vec{F}_{\mathrm{T}_1\mathrm{T}_3} \cdot \hat{R}_{\mathrm{r}} \tag{S49}$$

with

$$\vec{F}_{\mathrm{T}_1\mathrm{T}_3} = -\frac{1}{E_{\mathrm{T}_3} - E_{\mathrm{T}_1}} \frac{\partial V_{\mathrm{T}_1\mathrm{T}_3}}{\partial \vec{X}} \tag{S50}$$

We chose the ν_{106} mode at $\omega = 1279$ cm^{-1} for R_{r}. With this, $C_{\mathrm{r}} = 1.136 \times 10^{-4}$ a.u. was obtained. With the oscillation of R_{r} in time, the root-mean-squared value of the T_1–T_3 coupling due to this non-Condon effect, namely $\sqrt{|C_{\mathrm{r}} R_{\mathrm{r}}|^2}$ in the average sense, was ∼250 cm^{-1} during the trajectory durations. To emphasize the importance of the fluctuating non-Condon nature of this coupling, we additionally prepared a fictitious model system with $C_{\mathrm{r}} = 0$ but a relatively strong and non-fluctuating coupling $V_{\mathrm{T}_1\mathrm{T}_3} = 500$ cm^{-1}. This is equivalent to replacing $C_{\mathrm{r}} R_{\mathrm{r}}$ with $V_{\mathrm{T}_1\mathrm{T}_3}$ in eq S45.

Supporting Information Tables

Table S1: Normal modes of DABNA with major contributions to k_{SV} at different ΔE_{ST} values.

ΔE_{ST} (eV)	k_{SV} (10^4 s^{-1})[a]	dominant normal modes[b]
0.148	1.95 (89%)	ν_{106} (74.8%, 0.159)
0.162	1.38 (97%)	ν_{116} (60.9%, 0.174), ν_{118} (23.9%, 0.177)
0.167	2.12 (100%)	ν_{118} (85.1%, 0.177), ν_{116} (9.6%, 0.174)

[a] Diagonal contribution to total k_{SV} of eq S6 ($\equiv \sum_{\nu} [k_{SV}]_{\nu\nu} / k_{SV}$) are given in parentheses.
[b] Contributions within the diagonal in percentage and vibrational frequencies in eV units are given in parentheses. The normal mode motions are pictorially represented in Figure S3.

Table S2: Electronic state energies of DABNA from SCS-CC2 and SCS-ADC(2) calculations.[a]

N	S_N (eV)[b]	T_N (eV)[b]	$\Delta E_{S_N S_1}$ (eV)	$\Delta E_{T_N T_1}$ (eV)
1	3.044	2.908		
	(3.212)	(3.068)		
2	3.938	3.494	0.894	0.586
3	4.086	3.637	1.042	0.729
4	4.370	3.724	1.326	0.816
5	4.740	3.996	1.696	1.088
6	4.798	4.078	1.754	1.170
7	4.818	4.084	1.774	1.176
8	4.839	4.085	1.795	1.177
9	4.946	4.304	1.902	1.396
10	4.949	4.401	1.905	1.493
11	4.998	4.598	1.954	1.690
12	5.174	4.740	2.130	1.832
13	5.246	4.794	2.202	1.886
14	5.251	4.852	2.207	1.944
15	5.321	4.879	2.277	1.971
16	5.684	4.897	2.639	1.989
17	5.763	4.899	2.718	1.991
18	5.945	4.903	2.900	1.995
19	6.036	4.949	2.992	2.041
20	6.055	5.118	3.010	2.210

[a] Vertical transition energies in reference to the S_0 state energy at the S_1 state equilibrium geometry. First-excited states were obtained with the SCS-CC2 calculations, upon which all other energies were obtained via the excited-state energy gaps with the SCS-ADC(2) calculations. [b] Numbers in parentheses are the SCS-CC2 adiabatic energies obtained with ground and excited state geometry optimizations at the SCS-MP2 and the SCS-ADC(2) levels, respectively.

Table S3: Energy gaps (eV) between excited states estimated with various levels of theory.[a]

		ΔE_{ST}				ΔE_{TT}[b]	
molecule	basis	ω*B97X[c]	SCS-ADC(2)	SCS-CC2	expt.[d]	ω*B97X[c]	SCS-ADC(2)
DABNA	SVP	0.372	0.130	0.145	0.15 (EtOH)	0.778	0.729
	TZVPP	0.371	0.130	0.144			
TBN-TPA	SVP	0.461	0.127	0.140	0.14 (Toluene)	0.719	0.660
	TZVPP	0.444	0.125	0.137			
TABNA	SVP	0.605	0.153	0.164		0.457	0.412
	TZVPP	0.574	0.152	0.161			

[a] Optimized structures from the SCS-ADC(2)/SVP level of theory are used. [b] T_1/T_3 energy gaps. See the main text for details. [c] Optimal ω-values are: 0.147 (DABNA), 0.113 (TBN-TPA), 0.138 (TABNA). [d] Literature values measured in solution phase.

Table S4: Root-mean-squared deviations in Å between S_1 and T_1 geometries for various emitters based on multiple-resonance and donor–acceptor structures.

emitter	type	rmsd
DABNA	MR	0.010
TBN-TPA	MR	0.036
TABNA	MR	0.047
PTZ-DBTO2[a]	DA	0.078
4CzPN[b]	DA	0.540
4CzIPN[b]	DA	0.542
4CzTPN[b]	DA	0.591
Cz-4-PN[b]	DA	0.728
Cz-3-PN[b]	DA	0.784
3CzPN[b]	DA	0.929
2CzPN[b]	DA	0.972

Optimized geometries were obtained at: [a] the SCS-ADC(2)/def2-TZVPP (ref S1) or [b] the ω^*B97X/6-31G(d) level of theory (ref S19).

Table S5: Optimized geometries of the S_1 and the T_1 states obtained at the SCS-ADC(2)/SVP level of theory in Cartesian coordinates (Å).

	S_1 state			T_1 state		
atom	X	Y	Z	X	Y	Z
			DABNA			
C	−4.036178	3.091585	0.466263	−4.039219	3.088518	0.453151
C	−3.860253	1.716610	0.237155	−3.861540	1.717316	0.230237
C	−2.562148	1.170277	0.145986	−2.561838	1.169612	0.140326
C	−1.391760	2.004555	0.200344	−1.391468	2.003819	0.190524
C	−1.623804	3.373689	0.489476	−1.626830	3.376035	0.475717
C	−2.913777	3.915704	0.604449	−2.913000	3.914023	0.587989
B	0.000014	1.346646	0.000150	0.000007	1.345652	−0.000265
C	0.000006	−0.178961	0.000078	−0.000002	−0.174089	−0.000102
C	1.391796	2.004559	−0.199982	1.391497	2.003770	−0.191131
C	−1.210883	−0.919105	−0.010784	−1.211394	−0.918018	−0.009332
C	−1.213321	−2.343607	−0.019005	−1.211325	−2.337916	−0.016358
C	−0.000005	−3.047966	−0.000074	−0.000023	−3.046089	0.000233
C	1.213314	−2.343620	0.018938	1.211288	−2.337931	0.016663
C	1.210889	−0.919117	0.010860	1.211378	−0.918034	0.009294
C	2.562179	1.170270	−0.145657	2.561847	1.169539	−0.140910
C	3.860275	1.716553	−0.237245	3.861574	1.717260	−0.230367
C	4.036179	3.091429	−0.466962	4.039309	3.088659	−0.452015
C	2.913767	3.915568	−0.604935	2.913123	3.914036	−0.587903
C	1.623807	3.373616	−0.489504	1.626924	3.376044	−0.475988
N	−2.425813	−0.228674	−0.017226	−2.428403	−0.228969	−0.017301
N	2.425825	−0.228697	0.017403	2.428396	−0.229003	0.017056
C	−3.628012	−1.006432	−0.108370	−3.630369	−1.007658	−0.105706
C	3.628014	−1.006477	0.108493	3.630355	−1.007688	0.105608
C	4.164225	−1.297517	1.369778	4.168162	−1.300206	1.365813
C	5.332776	−2.065091	1.459697	5.337198	−2.067263	1.453236
C	5.958704	−2.534110	0.295730	5.961725	−2.534640	0.287867
C	5.415847	−2.235176	−0.963027	5.416996	−2.234604	−0.969733
C	4.248313	−1.468492	−1.061067	4.248500	−1.469011	−1.065244
C	−4.248266	−1.468602	1.061152	−4.248558	−1.468695	1.065236
C	−5.415827	−2.235238	0.963059	−5.417094	−2.234247	0.969871
C	−5.958738	−2.533998	−0.295715	−5.961828	−2.534511	−0.287672
C	−5.332850	−2.064832	−1.459646	−5.337237	−2.067448	−1.453133
C	−4.164283	−1.297291	−1.369672	−4.168151	−1.300450	−1.365858
H	−5.047375	3.502313	0.537425	−5.049814	3.500152	0.524525
H	−4.739628	1.077334	0.154609	−4.739503	1.075751	0.150254
H	−0.765194	4.033423	0.627416	−0.769818	4.037474	0.613517
H	−3.037671	4.983336	0.810958	−3.038214	4.982136	0.791683
H	−2.152894	−2.896526	−0.038498	−2.151796	−2.889859	−0.034359
H	−0.000010	−4.140669	−0.000123	−0.000031	−4.138403	0.000358
H	2.152882	−2.896550	0.038366	2.151751	−2.889884	0.034793
H	4.739658	1.077322	−0.154437	4.739498	1.075493	−0.151586
H	5.047368	3.502042	−0.538903	5.049927	3.500670	−0.520851
H	3.037639	4.983190	−0.811509	3.038381	4.981929	−0.792721
H	0.765180	4.033333	−0.627421	0.769945	4.037573	−0.613569
H	3.661602	−0.918625	2.263690	3.666988	−0.922157	2.260863
H	5.756419	−2.296300	2.440899	5.761861	−2.300023	2.433604
H	6.870748	−3.132532	0.369051	6.874153	−3.132686	0.359252
H	5.904434	−2.599341	−1.871012	5.904674	−2.597139	−1.878828
H	3.810734	−1.220353	−2.031873	3.808885	−1.220884	−2.035108
H	−3.810625	−1.220626	2.031973	−3.808941	−1.220390	2.035053
H	−5.904394	−2.599501	1.871016	−5.904793	−2.596581	1.879035
H	−6.870789	−3.132403	−0.369079	−6.874318	−3.132476	−0.358941
H	−5.756541	−2.295897	−2.440861	−5.761891	−2.300404	−2.433458
H	−3.661692	−0.918287	−2.263554	−3.666904	−0.922679	−2.260984
			TBN-TPA			
C	5.205880	−3.749045	−1.025425	5.203962	−3.747109	−1.040369
C	3.824768	−3.654225	−0.809870	3.826710	−3.650769	−0.829166
C	3.227787	−2.405530	−0.539167	3.228272	−2.402746	−0.551478
C	4.031426	−1.222860	−0.391065	4.030955	−1.219000	−0.393657
C	5.413512	−1.371053	−0.673446	5.416636	−1.369297	−0.676313
C	6.027631	−2.604894	−0.973593	6.026325	−2.597479	−0.980337
B	3.330698	0.105483	0.014934	3.331779	0.105942	0.012484
C	1.808077	0.052375	0.004252	1.810344	0.052450	0.002320
C	3.932512	1.480807	0.426042	3.931749	1.477318	0.425212
C	1.102377	−1.159715	−0.214114	1.104478	−1.159096	−0.221924

C	−0.315823	−1.202015	−0.286908	−0.309495	−1.200234	−0.291506
C	−1.065078	−0.042969	−0.010799	−1.058784	−0.043773	−0.011941
C	−0.394829	1.160643	0.277205	−0.389055	1.157945	0.278784
C	1.021685	1.216663	0.200354	1.023180	1.215440	0.206820
C	3.049411	2.608957	0.544310	3.048754	2.605981	0.556316
C	3.555149	3.898453	0.808150	3.555146	3.894481	0.830637
C	4.921958	4.088286	1.050090	4.918064	4.085782	1.068076
C	5.818686	3.000583	1.031794	5.816696	2.993155	1.037766
C	5.295181	1.724602	0.735279	5.297949	1.723571	0.734751
N	1.827923	−2.340267	−0.391275	1.829475	−2.341038	−0.405502
N	1.661588	2.447102	0.371150	1.661690	2.447327	0.384781
C	1.070300	−3.557185	−0.417391	1.071082	−3.557681	−0.433532
C	0.814116	3.603257	0.350415	0.813054	3.603028	0.368220
C	0.391308	4.114182	−0.881069	0.398649	4.123504	−0.861993
C	−0.550186	5.151881	−0.920630	−0.545812	5.158472	−0.899910
C	−1.089356	5.696252	0.260497	−1.096565	5.690210	0.281598
C	−0.613797	5.187489	1.489829	−0.628971	5.172454	1.510098
C	0.325544	4.153874	1.543640	0.313351	4.141338	1.562248
C	0.638121	−4.102535	−1.630223	0.627984	−4.094447	−1.646080
C	−0.182676	−5.239300	−1.628659	−0.196233	−5.228854	−1.644819
C	−0.588499	−5.850783	−0.426457	−0.594938	−5.845743	−0.443122
C	−0.115949	−5.292198	0.781455	−0.110324	−5.296449	0.764251
C	0.701943	−4.159194	0.794160	0.710888	−4.165956	0.777252
C	7.526544	−2.739519	−1.258611	7.524584	−2.732928	−1.266082
C	7.298943	3.239031	1.345163	7.296314	3.232515	1.351333
C	8.131502	1.952714	1.251295	8.132867	1.949758	1.247858
C	7.427337	3.797318	2.775614	7.423334	3.781412	2.785638
C	7.873846	4.256167	0.340522	7.866280	4.258557	0.352798
C	8.269817	−1.403023	−1.124703	8.270720	−1.398560	−1.129101
C	7.720729	−3.261789	−2.695230	7.716468	−3.252132	−2.704221
C	8.147140	−3.734792	−0.259302	8.142479	−3.732268	−0.269001
C	−1.514691	−7.070371	−0.380621	−1.526819	−7.060993	−0.396778
C	−0.779871	−8.241917	0.297778	−0.792601	−8.240104	0.269016
C	−1.952437	−7.518471	−1.782067	−1.978054	−7.498759	−1.797203
C	−2.775976	−6.708914	0.427602	−2.779727	−6.697643	0.423668
C	−2.175582	6.776477	0.259891	−2.188021	6.765211	0.281438
C	−3.432195	6.209994	0.949948	−3.448611	6.185094	0.952661
C	−2.561462	7.206893	−1.162275	−2.561865	7.208750	−1.139918
C	−1.671405	8.015065	1.023745	−1.697854	7.998124	1.063338
C	−3.313509	0.861783	−0.609314	−3.307941	0.849440	−0.627121
C	−4.665238	0.503162	−0.369425	−4.660609	0.497351	−0.380403
C	−4.638293	−0.727277	0.395153	−4.634253	−0.721268	0.402722
C	−3.271498	−1.047772	0.602268	−3.266888	−1.036608	0.616626
C	−5.648729	−1.549096	0.930925	−5.643707	−1.537097	0.949789
C	−5.310535	−2.690317	1.669682	−5.304136	−2.667602	1.704253
C	−3.929595	−2.976855	1.867157	−3.922767	−2.949225	1.907279
C	−2.905488	−2.181445	1.352532	−2.899639	−2.159889	1.381888
C	−2.997859	2.007204	−1.364751	−2.989974	1.984805	−1.396804
C	−4.055847	2.777279	−1.848782	−4.046321	2.750189	−1.891319
C	−5.423125	2.452847	−1.617122	−5.414343	2.431960	−1.654199
C	−5.710933	1.299120	−0.876068	−5.704613	1.288702	−0.898017
C	−6.359247	−3.629225	2.278400	−6.351632	−3.600627	2.324071
C	−6.175655	−5.045029	1.699959	−6.164391	−5.023530	1.764368
N	−2.476207	−0.081955	−0.014505	−2.472006	−0.083008	−0.016206
C	−7.791887	−3.168979	1.974222	−7.784909	−3.147613	2.012121
C	−6.182097	−3.671119	3.808214	−6.176594	−3.622270	3.854549
C	−6.512059	3.364027	−2.196817	−6.501260	3.338866	−2.244337
C	−7.923319	2.869323	−1.849740	−7.913671	2.851935	−1.890993
C	−6.380132	3.405480	−3.731239	−6.370155	3.362225	−3.779207
C	−6.348074	4.785978	−1.627604	−6.333511	4.766975	−1.691735
H	5.631272	−4.733850	−1.237120	5.630813	−4.729950	−1.256328
H	3.215115	−4.556723	−0.875817	3.214823	−4.551237	−0.902860
H	6.025701	−0.471730	−0.646628	6.030105	−0.471202	−0.646391
H	−0.839563	−2.119729	−0.551877	−0.834329	−2.118852	−0.552117
H	−0.981134	2.040426	0.539150	−0.977027	2.038310	0.535916
H	2.884149	4.758226	0.846912	2.881388	4.751640	0.879889
H	5.276788	5.101942	1.255492	5.273759	5.097196	1.280919
H	5.966889	0.868353	0.732706	5.971400	0.869006	0.726786
H	0.788158	3.680311	−1.803562	0.803624	3.698673	−1.785117
H	−0.870506	5.520072	−1.896545	−0.860201	5.533661	−1.875031
H	−0.999174	5.588209	2.431002	−1.023626	5.563103	2.451629
H	0.663570	3.748706	2.501684	0.644783	3.728567	2.519341
H	0.932112	−3.624835	−2.569196	0.915331	−3.611541	−2.584434
H	−0.515238	−5.634958	−2.589506	−0.538004	−5.617450	−2.605292

H	−0.396421	−5.742016	1.737530	−0.385094	−5.750766	1.719802
H	1.053959	−3.726824	1.735281	1.070566	−3.739649	1.718198
H	8.092832	1.520687	0.239951	8.094487	1.524595	0.233652
H	9.185307	2.178528	1.482099	9.186048	2.177815	1.479081
H	7.785670	1.191270	1.967411	7.790416	1.182454	1.959253
H	6.895830	4.754780	2.885182	6.889749	4.736730	2.902445
H	7.005530	3.088447	3.506011	7.004003	3.066195	3.511231
H	8.488132	3.965111	3.027933	8.483906	3.949775	3.038015
H	7.359858	5.227027	0.403834	7.350346	5.227733	0.423760
H	8.945326	4.426417	0.540161	8.937570	4.429551	0.552169
H	7.769359	3.882042	−0.690557	7.761252	3.891362	−0.680708
H	8.180372	−0.992686	−0.107521	8.182824	−0.990814	−0.110808
H	9.341068	−1.554710	−1.334928	9.341404	−1.552372	−1.340413
H	7.890091	−0.653315	−1.835999	7.892243	−0.646275	−1.838270
H	7.255588	−4.249785	−2.832300	7.250294	−4.239149	−2.843864
H	7.268104	−2.568782	−3.422393	7.264608	−2.556461	−3.429285
H	8.795198	−3.355146	−2.927463	8.790706	−3.345959	−2.936773
H	7.700621	−4.736316	−0.350436	7.694658	−4.732845	−0.362915
H	9.231464	−3.829854	−0.438481	9.226605	−3.828120	−0.448254
H	7.996776	−3.387690	0.775553	7.992460	−3.387522	0.766685
H	−0.487907	−7.995724	1.330079	−0.491061	−8.001283	1.300297
H	−1.431060	−9.130842	0.333545	−1.448067	−9.125851	0.305069
H	0.132837	−8.504469	−0.260750	0.114191	−8.504200	−0.298370
H	−2.506743	−6.724573	−2.306456	−2.532436	−6.699022	−2.312545
H	−1.091656	−7.813495	−2.402213	−1.123807	−7.794635	−2.425940
H	−2.617977	−8.391833	−1.696576	−2.647398	−8.369166	−1.711365
H	−3.289880	−5.841571	−0.016238	−3.292902	−5.825169	−0.010895
H	−3.477589	−7.559418	0.441896	−3.485451	−7.544711	0.438777
H	−2.531345	−6.457621	1.471174	−2.525541	−6.453477	1.466624
H	−3.234134	5.945474	1.999970	−3.259533	5.909458	2.001492
H	−4.244371	6.955793	0.935923	−4.264037	6.927335	0.939153
H	−3.783321	5.304523	0.429750	−3.790489	5.284037	0.418755
H	−1.703618	7.631290	−1.707111	−1.700497	7.642155	−1.671983
H	−2.963322	6.362035	−1.742988	−2.954913	6.368458	−1.733146
H	−3.344098	7.980299	−1.112373	−3.347998	7.978559	−1.089532
H	−0.762576	8.420739	0.551014	−0.786268	8.413204	0.604253
H	−2.442649	8.802797	1.022693	−2.472958	8.782034	1.062515
H	−1.433676	7.778859	2.072043	−1.469773	7.752246	2.111552
H	−6.692239	−1.277088	0.759566	−6.687635	−1.269885	0.773278
H	−3.643957	−3.857353	2.449551	−3.636561	−3.821350	2.501953
H	−1.860313	−2.436470	1.540343	−1.853725	−2.409859	1.573134
H	−1.965471	2.290434	−1.579672	−1.956495	2.262093	−1.615014
H	−3.808727	3.665312	−2.437846	−3.797811	3.630092	−2.491949
H	−6.741978	0.998220	−0.679400	−6.736377	0.993635	−0.696156
H	−5.181102	−5.453602	1.933637	−5.169057	−5.426786	2.004144
H	−6.930990	−5.731950	2.117511	−6.918545	−5.706750	2.190127
H	−6.287481	−5.032548	0.603713	−6.275205	−5.025497	0.667950
H	−7.992718	−2.169341	2.389868	−7.988310	−2.142945	2.414161
H	−7.986844	−3.141949	0.890853	−7.978553	−3.135318	0.928253
H	−8.509491	−3.871492	2.427510	−8.501621	−3.845575	2.473835
H	−6.294419	−2.663082	4.238432	−6.291928	−2.608957	4.271371
H	−6.940216	−4.329431	4.264820	−6.933755	−4.276414	4.318742
H	−5.189448	−4.052422	4.092285	−5.183398	−3.997331	4.144930
H	−8.084734	2.838441	−0.760958	−8.074867	2.834613	−0.801885
H	−8.671162	3.553596	−2.281530	−8.659999	3.532732	−2.330889
H	−8.112054	1.864758	−2.259044	−8.104866	1.842899	−2.287970
H	−5.405438	3.809637	−4.044588	−5.394609	3.760163	−4.097790
H	−6.480222	2.393640	−4.155481	−6.473025	2.345745	−4.191526
H	−7.166761	4.043834	−4.167531	−7.155413	3.997445	−4.222551
H	−5.372259	5.220291	−1.892906	−5.356178	5.195226	−1.961468
H	−7.132899	5.451783	−2.024458	−7.116163	5.430524	−2.096659
H	−6.426441	4.774899	−0.528581	−6.412433	4.768799	−0.592693

TABNA

C	−2.056272	3.744545	−0.079795	−2.032107	3.730135	−0.130047
C	−2.801176	2.543014	−0.015979	−2.792749	2.536239	−0.048015
C	−2.117953	1.301199	0.098656	−2.132234	1.303579	0.087376
C	−0.708907	1.290985	0.261681	−0.721441	1.304985	0.230701
C	0.038843	2.485602	0.099463	0.034680	2.498635	0.072514
C	−0.642623	3.728390	−0.015386	−0.632007	3.734345	−0.064801
B	0.000623	−0.001145	0.440491	−0.006157	0.000502	0.407045
C	−0.770863	−1.279580	0.251056	−0.776561	−1.272377	0.231078
C	1.493441	−0.036116	0.252043	1.474057	−0.031272	0.242737
C	−2.176393	−1.214557	0.076949	−2.185291	−1.210417	0.087178
C	−2.912472	−2.404870	−0.090516	−2.897638	−2.414348	−0.049754

C	−2.204803	−3.620765	−0.158818	−2.189234	−3.639998	−0.132882
C	−0.803084	−3.688051	−0.058274	−0.790684	−3.703473	−0.067535
C	−0.064633	−2.493993	0.101244	−0.072346	−2.496799	0.072005
C	2.139218	−1.283766	0.102237	2.129628	−1.274848	0.080371
C	3.543219	−1.301308	−0.056352	3.539445	−1.304759	−0.061861
C	4.238830	−0.082405	−0.155804	4.257042	−0.092007	−0.136078
C	3.592529	1.167268	−0.087872	3.590658	1.151649	−0.062001
C	2.193020	1.184862	0.078662	2.181398	1.183081	0.080650
N	−2.798692	0.064770	0.116289	−2.815631	0.060158	0.148308
N	1.355847	−2.469048	0.178012	1.352000	−2.455456	0.112918
C	−4.227567	0.096669	0.014341	−4.239457	0.090405	0.041547
C	2.040704	−3.716253	0.062867	2.043445	−3.706904	0.026349
C	2.332623	−4.246873	−1.204744	2.340159	−4.254711	−1.230496
C	3.004645	−5.470936	−1.309892	3.016766	−5.478478	−1.306218
C	3.385703	−6.166517	−0.152677	3.391686	−6.149574	−0.132789
C	3.093233	−5.634913	1.111404	3.089343	−5.596120	1.119701
C	2.421057	−4.410299	1.221442	2.412669	−4.372269	1.203480
C	−4.835525	0.151299	−1.248503	−4.850853	0.105128	−1.222697
C	−6.232710	0.182362	−1.339179	−6.247607	0.134538	−1.319959
C	−7.014734	0.156769	−0.174853	−7.034006	0.149530	−0.158366
C	−6.398677	0.100390	1.083717	−6.420613	0.135161	1.102502
C	−5.001569	0.069913	1.182628	−5.023503	0.105544	1.204870
N	1.447361	2.396498	0.117851	1.455886	2.395862	0.113272
C	2.187014	3.619485	0.016537	2.200494	3.616257	0.026282
C	2.468172	4.161747	−1.246086	2.517707	4.152381	−1.230597
C	3.191468	5.357576	−1.336152	3.246610	5.345762	−1.306686
C	3.631162	6.004089	−0.171431	3.653029	5.998668	−0.133528
C	3.347253	5.453924	1.086910	3.329790	5.457434	1.119122
C	2.623633	4.258384	1.185212	2.600960	4.263958	1.203149
H	−2.580909	4.700198	−0.156821	−2.561315	4.681701	−0.237609
H	−3.889753	2.581864	−0.095099	−3.880941	2.591331	−0.123100
H	−0.091420	4.667906	−0.094314	−0.085866	4.675070	−0.156007
H	−3.998044	−2.400807	−0.203317	−3.987198	−2.422309	−0.125121
H	−2.767591	−4.550568	−0.286894	−2.758858	−4.567750	−0.241437
H	−0.305655	−4.657233	−0.134804	−0.284380	−4.666103	−0.159944
H	4.094110	−2.241111	−0.133155	4.075579	−2.252081	−0.151664
H	5.325591	−0.106479	−0.282366	5.344970	−0.114428	−0.236283
H	4.171754	2.085434	−0.200410	4.167343	2.074807	−0.152360
H	2.027516	−3.690299	−2.095307	2.035926	−3.716681	−2.132412
H	3.232235	−5.884144	−2.296746	3.251066	−5.910373	−2.283151
H	3.910300	−7.122329	−0.236585	3.919324	−7.105156	−0.194907
H	3.389675	−6.175985	2.014526	3.380179	−6.119655	2.034603
H	2.183411	−3.978020	2.197066	2.164395	−3.923755	2.169018
H	−4.207212	0.166462	−2.143208	−4.221023	0.093566	−2.116563
H	−6.712754	0.225100	−2.320816	−6.724734	0.145772	−2.304114
H	−8.105346	0.179929	−0.248773	−8.124507	0.172337	−0.236268
H	−7.008010	0.079532	1.991488	−7.032479	0.147238	2.008969
H	−4.499956	0.024505	2.152906	−4.525022	0.093833	2.177806
H	2.119444	3.639382	−2.141089	2.188100	3.629321	−2.132402
H	3.413922	5.785506	−2.317613	3.497149	5.768185	−2.283742
H	4.196077	6.937311	−0.244858	4.221530	6.930507	−0.195924
H	3.690679	5.957141	1.994981	3.644941	5.966973	2.033882
H	2.392436	3.810451	2.155274	2.335649	3.825572	2.168815

Table S6: Harmonic vibrational frequencies (cm^{-1}) of the S_1 and the T_1 states calculated at the SCS-ADC(2)/SVP level of theory.[a]

mode	S_1	T_1	mode	S_1	T_1	mode	S_1	T_1	mode	S_1	T_1
					DABNA						
1	13.6	14.7	40	547.0	546.6	79	983.6	983.5	118	1426.0	1325.4
2	20.3	20.4	41	549.5	547.8	80	984.3	984.3	119	1430.1	1425.4
3	38.5	39.9	42	586.8	584.9	81	1008.3	1008.2	120	1440.5	1440.6
4	42.1	42.9	43	599.2	603.0	82	1012.6	1012.8	121	1440.6	1440.7
5	50.2	50.3	44	608.0	608.0	83	1022.5	1023.7	122	1460.4	1460.9
6	61.1	62.9	45	610.8	613.5	84	1030.4	1033.2	123	1469.4	1455.6
7	68.8	68.9	46	612.3	611.8	85	1041.0	1043.4	124	1488.9	1489.4
8	72.6	72.3	47	617.8	610.3	86	1058.8	1058.9	125	1492.0	1485.0
9	82.8	82.4	48	622.1	623.5	87	1058.8	1058.9	126	1493.8	1509.0
10	116.4	116.5	49	635.8	633.6	88	1061.4	1065.8	127	1522.7	1503.0
11	163.0	165.2	50	636.1	634.0	89	1079.1	1081.1	128	1549.5	1525.0
12	165.6	166.9	51	663.8	663.6	90	1093.7	1097.8	129	1554.1	1539.3
13	189.5	189.5	52	698.6	700.7	91	1127.8	1133.5	130	1555.7	1559.4
14	195.9	198.7	53	700.8	702.8	92	1134.8	1074.9	131	1576.6	1582.1
15	201.2	201.4	54	705.2	706.6	93	1135.4	1135.5	132	1599.6	1599.8
16	219.9	221.5	55	707.5	704.1	94	1135.4	1135.5	133	1599.8	1600.0
17	232.2	231.1	56	724.2	724.9	95	1138.7	1137.4	134	1610.0	1608.9
18	233.5	234.4	57	742.3	739.1	96	1139.3	1127.7	135	1610.4	1610.9
19	253.0	253.5	58	794.4	798.0	97	1144.0	1144.4	136	3098.0	3098.4
20	266.1	266.5	59	809.9	814.7	98	1146.4	1145.3	137	3099.0	3099.7
21	301.0	303.8	60	817.6	818.0	99	1168.9	1173.2	138	3108.3	3108.6
22	331.9	329.7	61	817.6	818.0	100	1174.1	1177.0	139	3108.3	3108.6
23	358.0	357.0	62	820.0	840.4	101	1201.7	1210.1	140	3114.4	3115.8
24	374.8	376.1	63	837.8	836.0	102	1228.8	1224.3	141	3115.4	3115.7
25	383.8	384.1	64	853.2	860.7	103	1240.0	1237.5	142	3115.4	3115.7
26	385.3	385.5	65	855.5	857.9	104	1249.3	1234.4	143	3116.0	3117.0
27	394.7	395.6	66	861.0	862.1	105	1262.5	1265.0	144	3119.8	3121.9
28	397.5	398.4	67	861.4	864.6	106	1279.3	1254.9	145	3123.4	3123.7
29	410.4	411.4	68	874.0	874.4	107	1284.6	1284.8	146	3123.4	3123.7
30	425.8	427.0	69	880.0	880.3	108	1284.7	1284.9	147	3127.9	3129.9
31	433.3	434.8	70	887.3	887.0	109	1295.6	1297.6	148	3128.8	3129.1
32	443.9	438.9	71	899.0	900.2	110	1297.0	1315.7	149	3128.8	3129.1
33	454.6	455.0	72	902.4	899.8	111	1336.8	1336.6	150	3134.8	3135.1
34	456.8	459.2	73	904.8	912.4	112	1336.9	1336.6	151	3134.9	3135.1
35	471.8	471.8	74	913.6	922.2	113	1355.5	1362.6	152	3143.6	3144.3
36	481.1	480.8	75	934.5	934.8	114	1366.6	1348.0	153	3144.0	3144.4
37	497.6	498.5	76	934.5	934.8	115	1392.4	1374.3	154	3145.8	3148.6
38	501.1	501.1	77	938.9	939.2	116	1401.9	1407.2	155	3147.8	3145.8
39	539.6	538.9	78	939.0	939.4	117	1420.1	1419.7	156	3150.8	3149.8
					TBN-TPA						
1	8.6	8.5	109	466.1	464.0	217	1071.8	1073.1	325	1461.3	1461.6
2	11.8	11.8	110	473.0	471.8	218	1077.8	1078.5	326	1461.7	1461.7
3	13.1	13.0	111	480.8	483.2	219	1090.6	1090.3	327	1462.4	1462.4
4	14.5	14.4	112	490.7	490.8	220	1093.1	1093.2	328	1462.6	1464.4
5	22.2	23.3	113	492.5	491.3	221	1093.4	1093.5	329	1462.6	1462.6
6	22.9	22.0	114	504.2	505.8	222	1100.2	1099.9	330	1463.0	1463.0
7	25.2	25.2	115	505.1	504.6	223	1105.0	1105.1	331	1463.5	1463.5
8	27.7	27.0	116	511.1	510.3	224	1105.6	1105.6	332	1471.5	1472.2
9	28.5	27.6	117	522.6	522.4	225	1112.7	1113.8	333	1473.0	1473.1
10	30.5	30.7	118	523.2	522.7	226	1120.3	1122.1	334	1473.6	1473.9
11	31.8	32.3	119	545.1	544.6	227	1125.3	1126.2	335	1474.1	1474.4
12	34.0	33.9	120	547.7	547.7	228	1131.9	1131.3	336	1474.8	1475.5
13	36.8	37.0	121	550.0	550.1	229	1143.7	1140.5	337	1476.2	1476.2
14	38.8	38.8	122	563.9	564.3	230	1150.5	1151.8	338	1477.3	1452.4
15	41.3	40.9	123	564.9	566.5	231	1158.7	1158.4	339	1478.8	1478.7
16	59.7	60.1	124	575.4	575.5	232	1159.2	1159.5	340	1492.5	1492.8
17	61.6	62.1	125	581.6	581.8	233	1179.5	1181.6	341	1504.3	1501.0
18	64.3	64.2	126	584.9	590.0	234	1194.8	1196.2	342	1506.5	1501.9
19	65.8	65.9	127	589.1	588.7	235	1199.3	1189.4	343	1515.7	1524.6
20	67.9	68.0	128	593.6	593.7	236	1212.4	1212.4	344	1528.9	1512.0
21	73.4	73.2	129	602.3	607.5	237	1215.0	1217.0	345	1530.8	1491.6
22	76.7	76.2	130	602.4	602.3	238	1216.2	1216.1	346	1543.6	1549.5
23	87.1	86.1	131	612.8	613.0	239	1216.5	1216.4	347	1562.2	1567.8
24	92.2	91.7	132	613.8	614.1	240	1216.6	1216.5	348	1570.5	1570.0
25	96.8	97.0	133	618.9	620.6	241	1217.7	1217.8	349	1571.3	1571.3
26	98.8	98.9	134	627.9	628.6	242	1218.3	1218.6	350	1578.8	1579.2
27	101.9	102.1	135	631.1	631.0	243	1219.8	1223.0	351	1579.3	1579.6
28	121.5	121.1	136	633.0	633.5	244	1220.3	1220.2	352	1582.4	1591.6
29	126.7	126.6	137	641.8	641.5	245	1220.5	1220.4	353	1614.3	1613.9
30	147.7	148.2	138	651.4	650.8	246	1221.0	1220.9	354	1615.9	1615.8

31	149.6	150.3	139	667.7	667.1	247	1221.6	1221.6	355	1616.5	1617.0
32	155.6	155.7	140	671.6	665.5	248	1228.2	1174.9	356	1636.9	1637.2
33	163.1	162.5	141	693.2	692.7	249	1230.5	1230.7	357	2956.1	2957.0
34	171.0	171.3	142	698.0	697.9	250	1231.5	1231.8	358	2956.2	2957.1
35	177.4	177.5	143	712.8	710.0	251	1237.1	1230.3	359	2956.7	2956.5
36	185.3	185.2	144	713.8	713.9	252	1250.5	1250.8	360	2956.9	2956.7
37	191.9	191.9	145	743.2	737.9	253	1258.6	1256.6	361	2957.8	2958.5
38	196.2	196.8	146	754.5	751.9	254	1261.0	1246.8	362	2958.0	2957.9
39	206.8	206.3	147	755.8	752.9	255	1275.4	1275.6	363	2958.0	2958.8
40	212.8	211.8	148	761.7	764.4	256	1278.0	1278.4	364	2958.1	2958.0
41	220.3	220.1	149	764.9	765.6	257	1278.8	1278.9	365	2958.6	2958.5
42	224.2	224.4	150	770.5	771.3	258	1280.4	1281.1	366	2959.0	2959.1
43	225.7	225.6	151	783.1	794.8	259	1281.2	1282.1	367	2960.0	2960.1
44	226.6	226.1	152	792.9	793.2	260	1281.6	1281.8	368	2960.1	2960.1
45	231.7	230.6	153	805.2	805.3	261	1283.2	1284.9	369	2963.3	2963.8
46	235.0	235.0	154	809.5	809.7	262	1284.6	1292.8	370	2963.5	2963.4
47	237.8	237.4	155	810.0	810.2	263	1291.2	1293.5	371	2963.6	2963.5
48	239.1	238.6	156	811.8	811.2	264	1296.6	1308.1	372	2964.0	2964.5
49	240.0	239.7	157	813.3	815.6	265	1303.1	1303.2	373	2964.5	2964.4
50	254.6	254.2	158	820.8	841.4	266	1305.6	1310.9	374	2965.0	2965.0
51	256.4	256.0	159	827.0	827.4	267	1332.3	1332.2	375	3051.6	3052.6
52	258.2	257.9	160	829.8	828.5	268	1333.0	1332.7	376	3051.8	3052.8
53	260.7	260.4	161	832.9	834.0	269	1342.5	1266.6	377	3051.9	3052.9
54	270.7	270.4	162	837.8	838.6	270	1347.1	1353.4	378	3052.0	3051.7
55	271.7	271.2	163	839.4	839.4	271	1351.9	1356.3	379	3052.2	3051.9
56	276.1	276.0	164	839.6	839.5	272	1357.7	1363.8	380	3052.4	3053.2
57	278.4	277.3	165	843.4	843.5	273	1360.4	1360.4	381	3053.3	3053.1
58	279.3	278.3	166	845.2	846.2	274	1360.5	1360.5	382	3053.4	3053.1
59	281.0	281.0	167	858.7	862.9	275	1361.3	1361.3	383	3056.7	3056.7
60	283.0	282.7	168	860.4	864.2	276	1361.4	1361.3	384	3056.7	3056.9
61	285.3	285.5	169	869.8	871.0	277	1361.5	1357.1	385	3057.2	3057.2
62	288.4	287.9	170	890.1	887.1	278	1362.8	1362.8	386	3057.4	3057.4
63	290.1	290.9	171	891.4	891.6	279	1363.7	1363.8	387	3057.9	3058.6
64	300.3	304.8	172	893.5	893.5	280	1364.0	1364.1	388	3058.6	3059.3
65	315.0	315.5	173	899.4	899.6	281	1364.5	1364.5	389	3059.4	3059.2
66	316.4	316.9	174	899.7	898.7	282	1365.2	1365.4	390	3059.7	3059.5
67	325.6	326.6	175	902.8	903.0	283	1365.9	1363.3	391	3063.0	3063.1
68	328.5	328.7	176	904.5	902.1	284	1368.3	1375.1	392	3063.5	3063.6
69	334.2	333.3	177	906.2	905.6	285	1373.8	1380.6	393	3065.2	3065.1
70	336.4	336.4	178	921.6	923.3	286	1379.9	1357.7	394	3065.9	3065.9
71	337.2	337.2	179	924.1	924.0	287	1385.9	1372.5	395	3066.2	3066.2
72	337.9	337.9	180	924.1	924.6	288	1388.6	1389.1	396	3066.3	3066.2
73	338.3	338.2	181	924.2	924.1	289	1389.6	1389.2	397	3068.0	3069.0
74	339.2	338.3	182	925.3	925.8	290	1389.8	1389.8	398	3068.5	3069.6
75	339.4	339.1	183	925.6	925.5	291	1390.4	1389.7	399	3068.6	3068.7
76	341.5	341.2	184	925.9	926.0	292	1391.5	1391.4	400	3068.8	3068.8
77	342.5	342.3	185	931.4	931.6	293	1391.5	1391.6	401	3069.0	3069.0
78	344.8	344.8	186	931.6	931.8	294	1393.5	1391.7	402	3069.0	3068.9
79	346.8	346.5	187	931.9	930.9	295	1402.5	1402.5	403	3069.5	3069.5
80	347.5	347.5	188	932.6	932.6	296	1402.6	1402.6	404	3070.0	3069.7
81	348.1	348.1	189	932.8	932.8	297	1427.2	1428.0	405	3070.6	3071.5
82	355.3	355.4	190	932.9	933.3	298	1431.6	1416.0	406	3070.6	3070.5
83	358.7	358.8	191	934.0	933.9	299	1434.3	1395.7	407	3071.0	3072.1
84	368.1	368.3	192	934.0	933.9	300	1437.6	1437.6	408	3071.1	3072.1
85	369.0	369.3	193	936.8	937.1	301	1438.0	1438.0	409	3071.7	3071.0
86	372.1	372.5	194	937.4	937.3	302	1438.4	1438.4	410	3073.8	3074.4
87	384.1	383.5	195	937.7	937.6	303	1438.6	1438.7	411	3104.1	3103.5
88	385.0	385.2	196	938.6	935.9	304	1439.2	1439.2	412	3107.2	3106.4
89	388.9	388.3	197	939.4	939.7	305	1439.3	1439.2	413	3107.7	3110.5
90	389.7	389.9	198	939.9	939.7	306	1440.0	1440.0	414	3107.9	3111.0
91	392.9	391.9	199	940.0	940.1	307	1440.9	1440.9	415	3109.7	3110.2
92	393.1	392.6	200	995.8	995.2	308	1440.9	1441.1	416	3111.2	3111.4
93	393.6	394.0	201	997.8	997.8	309	1441.0	1441.2	417	3113.3	3113.7
94	394.8	395.4	202	1005.3	1004.8	310	1441.9	1441.8	418	3115.6	3115.7
95	403.2	404.0	203	1017.2	1019.7	311	1442.8	1442.8	419	3124.9	3125.3
96	407.8	406.1	204	1020.1	1020.1	312	1444.5	1443.7	420	3126.2	3126.4
97	412.3	412.3	205	1020.3	1020.2	313	1445.0	1445.6	421	3126.8	3126.3
98	412.8	413.2	206	1020.3	1018.9	314	1445.5	1445.4	422	3128.4	3127.4
99	416.8	417.1	207	1020.6	1020.8	315	1445.9	1446.0	423	3129.6	3128.6
100	419.4	418.5	208	1021.3	1020.5	316	1446.6	1446.6	424	3130.6	3129.8
101	427.6	427.5	209	1022.7	1022.4	317	1447.2	1447.1	425	3134.1	3134.4
102	437.7	437.8	210	1023.6	1023.3	318	1456.8	1457.4	426	3135.7	3135.9
103	438.8	439.2	211	1023.8	1023.7	319	1458.4	1458.0	427	3143.0	3143.6
104	448.7	448.9	212	1024.2	1024.2	320	1458.4	1458.7	428	3144.3	3144.6
105	450.4	450.0	213	1024.6	1024.6	321	1459.2	1459.1	429	3153.9	3152.3
106	455.9	456.0	214	1024.9	1024.9	322	1459.4	1459.4	430	3154.9	3153.3
107	460.9	461.2	215	1025.0	1025.0	323	1459.6	1459.5	431	3155.0	3157.0
108	465.0	467.1	216	1058.3	1048.7	324	1460.0	1460.1	432	3175.8	3178.3

TABNA

1	18.5	18.9	48	547.1	546.8	95	983.7	981.2	142	1432.9	1400.1
2	21.3	24.0	49	548.6	535.1	96	984.2	984.2	143	1439.0	1440.1
3	25.5	22.7	50	568.0	570.3	97	995.3	1030.5	144	1440.0	1439.4
4	29.5	30.0	51	573.9	568.5	98	1001.0	987.6	145	1440.2	1439.9
5	32.3	34.3	52	584.4	916.5	99	1007.3	1010.7	146	1456.1	1460.3
6	33.5	32.8	53	605.1	605.9	100	1012.7	1012.8	147	1477.9	1485.8
7	47.9	48.3	54	607.5	607.1	101	1014.7	1008.8	148	1480.4	1488.3
8	48.1	46.7	55	610.1	603.1	102	1016.5	1013.3	149	1487.8	1388.2
9	61.2	62.6	56	610.2	610.8	103	1044.9	1043.5	150	1488.6	1485.2
10	71.6	71.6	57	611.2	611.3	104	1056.1	1058.3	151	1491.5	1492.6
11	84.4	85.5	58	614.3	609.0	105	1058.1	1056.5	152	1522.5	1501.1
12	86.6	83.7	59	633.7	636.8	106	1058.2	1058.2	153	1541.9	1507.3
13	182.4	198.3	60	639.8	646.3	107	1058.4	1053.4	154	1564.5	1555.4
14	183.5	182.7	61	646.1	641.5	108	1059.4	1035.6	155	1565.1	1564.4
15	189.8	188.8	62	652.8	699.1	109	1131.4	1111.8	156	1576.8	1524.0
16	198.1	124.9	63	686.2	705.7	110	1133.6	1135.1	157	1596.8	1599.2
17	202.5	202.0	64	699.4	666.8	111	1135.2	1135.1	158	1599.1	1597.4
18	209.8	212.7	65	703.3	694.9	112	1135.2	1133.8	159	1599.3	1599.1
19	213.2	207.7	66	705.9	682.7	113	1141.0	1101.0	160	1609.0	1608.3
20	230.5	257.2	67	722.0	720.6	114	1143.1	1142.4	161	1610.7	1612.6
21	241.5	233.2	68	736.3	736.2	115	1143.8	1144.1	162	1612.4	1611.0
22	245.7	247.5	69	738.3	747.7	116	1145.0	1144.2	163	3099.0	3103.2
23	247.2	245.9	70	746.6	726.9	117	1145.1	1213.5	164	3100.9	3114.7
24	260.9	261.3	71	811.7	822.7	118	1154.7	1156.7	165	3103.9	3108.0
25	291.5	323.1	72	812.0	864.6	119	1174.1	218.3	166	3107.5	3104.1
26	318.0	386.4	73	816.5	817.0	120	1183.2	1190.9	167	3107.6	3107.7
27	328.0	330.5	74	816.6	818.1	121	1189.4	1188.5	168	3111.5	3115.2
28	384.6	385.2	75	817.8	817.3	122	1201.2	1189.1	169	3114.6	3100.6
29	385.0	388.8	76	818.1	825.5	123	1226.3	1218.2	170	3115.0	3111.9
30	389.3	385.5	77	819.7	818.7	124	1239.8	1263.6	171	3115.0	3115.1
31	395.8	424.7	78	850.7	844.7	125	1266.6	1266.8	172	3120.8	3123.7
32	421.3	438.0	79	851.9	841.8	126	1271.9	1227.7	173	3123.3	3121.0
33	426.2	421.5	80	875.2	830.5	127	1280.6	1283.9	174	3123.3	3123.4
34	429.7	458.6	81	875.5	863.8	128	1284.0	1281.2	175	3126.4	3129.0
35	431.1	428.8	82	879.5	879.0	129	1284.1	1283.7	176	3128.7	3126.6
36	438.3	397.8	83	884.0	881.4	130	1287.7	1286.0	177	3128.7	3128.8
37	441.0	437.1	84	887.0	883.1	131	1327.6	1357.7	178	3130.2	3135.8
38	449.7	427.7	85	888.4	888.2	132	1330.9	1334.4	179	3130.7	3131.0
39	464.7	460.4	86	892.5	897.7	133	1333.7	1336.4	180	3131.2	3128.6
40	469.1	475.6	87	894.6	889.0	134	1336.8	1334.1	181	3132.1	3134.8
41	469.6	469.9	88	933.8	934.1	135	1336.9	1336.2	182	3134.3	3132.2
42	479.7	481.8	89	933.8	934.3	136	1366.6	1361.4	183	3134.5	3134.5
43	480.4	473.7	90	934.4	934.3	137	1367.8	1251.0	184	3135.4	3129.1
44	494.9	530.5	91	936.6	938.6	138	1388.0	1456.4	185	3135.9	3137.2
45	517.6	505.8	92	937.8	936.5	139	1397.3	1432.5	186	3136.7	3135.1
46	539.3	550.0	93	938.0	938.1	140	1412.6	1329.0			
47	545.3	542.0	94	980.7	983.0	141	1424.5	1431.9			

[a] Triplet modes are not sorted in frequencies but matched with singlet modes such that the normal mode vectors are maximally overlapping.

Table S7: Spin–orbit coupling between excited states of DABNA calculated at the ω*B97X level.

states[a]	rel. energies[b]	M = 0[c]	M = 1[c,d]	magnitude[c]
S_1/T_1	0.144/0	0.000i	0.053+0.000i	0.035
S_1/T_2	0.144/0.607	−0.708i	0.000+0.487i	0.561
S_1/T_3	0.144/0.778	1.593i	0.000−0.409i	0.804
S_1/T_4	0.144/0.896	0.000i	−0.163+0.000i	0.109
S_1/T_5	0.144/1.113	0.000i	−0.153+0.000i	0.102
S_1/T_6	0.144/1.353	−0.632i	0.000−0.145i	0.307
S_1/T_7	0.144/1.412	−0.137i	0.000+0.091i	0.106
S_1/T_8	0.144/1.431	0.000i	0.079−0.001i	0.053
S_1/T_9	0.144/1.433	−0.104i	0.000−0.109i	0.107
S_1/T_{10}	0.144/1.506	0.000i	0.187+0.000i	0.125
S_1/T_{11}	0.144/1.477	0.150i	0.000−1.461i	1.024
S_1/T_{12}	0.144/1.529	0.000i	0.843+0.000i	0.562
S_1/T_{13}	0.144/1.734	−0.373i	0.000+0.178i	0.243
S_1/T_{14}	0.144/1.726	−0.613i	0.000−0.186i	0.329
S_1/T_{15}	0.144/1.780	0.000i	0.150+0.000i	0.100
S_1/T_{16}	0.144/2.032	−0.085i	0.000+0.012i	0.036
S_1/T_{17}	0.144/2.037	0.000i	−0.049+0.000i	0.032
S_1/T_{18}	0.144/2.043	0.021i	0.000−0.170i	0.120
S_1/T_{19}	0.144/2.048	0.000i	0.023+0.000i	0.015
S_1/T_{20}	0.144/2.081	−0.202i	0.000+0.089i	0.127
S_2/T_1	0.980/0	0.000i	0.163+0.000i	0.108
S_3/T_1	1.025/0	0.607i	0.000−0.428i	0.487
S_4/T_1	1.022/0	−0.178i	0.000+1.370i	0.973
S_5/T_1	1.077/0	0.000i	−1.258+0.000i	0.839
S_6/T_1	1.237/0	1.609i	0.000−0.137i	0.627
S_7/T_1	1.359/0	−0.397i	0.000+0.319i	0.345
S_8/T_1	1.443/0	0.000i	0.256+0.000i	0.171
S_9/T_1	1.834/0	0.000i	0.025−0.001i	0.017
S_{10}/T_1	1.865/0	0.538i	0.001−0.437i	0.471
S_{11}/T_1	1.919/0	0.000i	0.156+0.000i	0.104
S_{12}/T_1	2.020/0	−0.853i	0.000+0.278i	0.470
S_{13}/T_1	2.148/0	0.000i	−0.171+0.000i	0.114
S_{14}/T_1	2.205/0	0.000i	0.115+0.000i	0.077
S_{15}/T_1	2.206/0	−0.068i	0.000−0.163i	0.131
S_{16}/T_1	2.314/0	0.000i	−0.309+0.000i	0.206
S_{17}/T_1	2.423/0	−0.328i	0.000−0.040i	0.136
S_{18}/T_1	2.482/0	−0.001i	0.335+0.001i	0.224
S_{19}/T_1	2.440/0	0.000i	−0.325−0.001i	0.217
S_{20}/T_1	2.491/0	−0.428i	0.001−0.863i	0.718

[a] Corresponding NTO pairs are depicted in Figure S4. [b] Relative energies in eV with respect to T_1. ΔE_{ST} from the SCS-CC2 level is adopted. [c] In cm^{-1} unit. [d] $SOC(M = -1) = -SOC(M = 1)^*$.

Table S8: Normal mode specific S_1–T_1 reorganization energies (λ) of DABNA.[a]

frequency	λ	frequency	λ	frequency	λ
20.32	0.13	636.07	0.04	1139.30	1.45
42.06	0.05	700.80	0.02	1144.04	0.01
72.57	0.23	705.22	1.15	1174.13	0.05
116.44	0.12	724.21	0.15	1201.72	0.14
165.57	0.01	809.88	0.01	1249.34	0.04
195.86	0.33	819.96	0.01	1262.49	0.02
201.23	0.26	853.23	0.02	1297.00	1.89
233.48	0.11	855.47	0.03	1366.63	9.30
252.97	0.05	874.03	0.37	1392.43	0.14
374.81	0.53	887.33	0.12	1430.09	5.22
385.30	0.01	899.01	1.85	1440.63	0.01
397.45	0.50	902.42	0.01	1460.37	1.28
410.39	1.30	904.84	0.03	1488.95	0.13
425.79	0.87	913.58	0.13	1493.79	0.34
433.31	0.02	934.51	0.02	1549.48	1.79
471.76	0.04	939.03	0.01	1576.58	1.86
497.58	0.05	1012.63	0.01	1610.38	0.02
539.63	0.03	1041.01	0.62	3098.99	0.02
546.98	0.26	1061.36	0.01	3119.83	0.04
608.04	0.01	1079.15	0.04	3150.76	0.03
612.31	0.10	1127.75	0.42		

[a] Both frequency and λ values are in cm^{-1} units.

Table S9: Dependence of the golden rule rate on the dephasing timescale of the damped Lorentzian for DABNA.

γ^a	k_{RISC} $(10^4\ \mathrm{s}^{-1})^b$
1 ps	2.00
10 ps	1.95
100 ps	1.95
1 ns	1.95
10 ns	1.95
100 ns	1.95

[a] The corresponding time correlation was monitored carefully for its decay to zero earlier than γ in all cases. [b] Rate values at $\Delta E_{\mathrm{ST}} = 0.148$ eV.

Supporting Information Figures

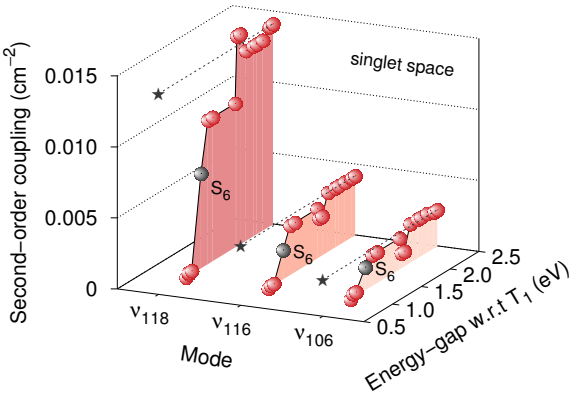

Figure S1: Convergence profiles of the sum-over-electronic-states expansion for each mode in the singlet manifold. The excited state with a dominant contribution (S_6) can be easily identified as marked with gray spheres. Convergence was reached with 20 excited states as denoted with dashed lines and stars.

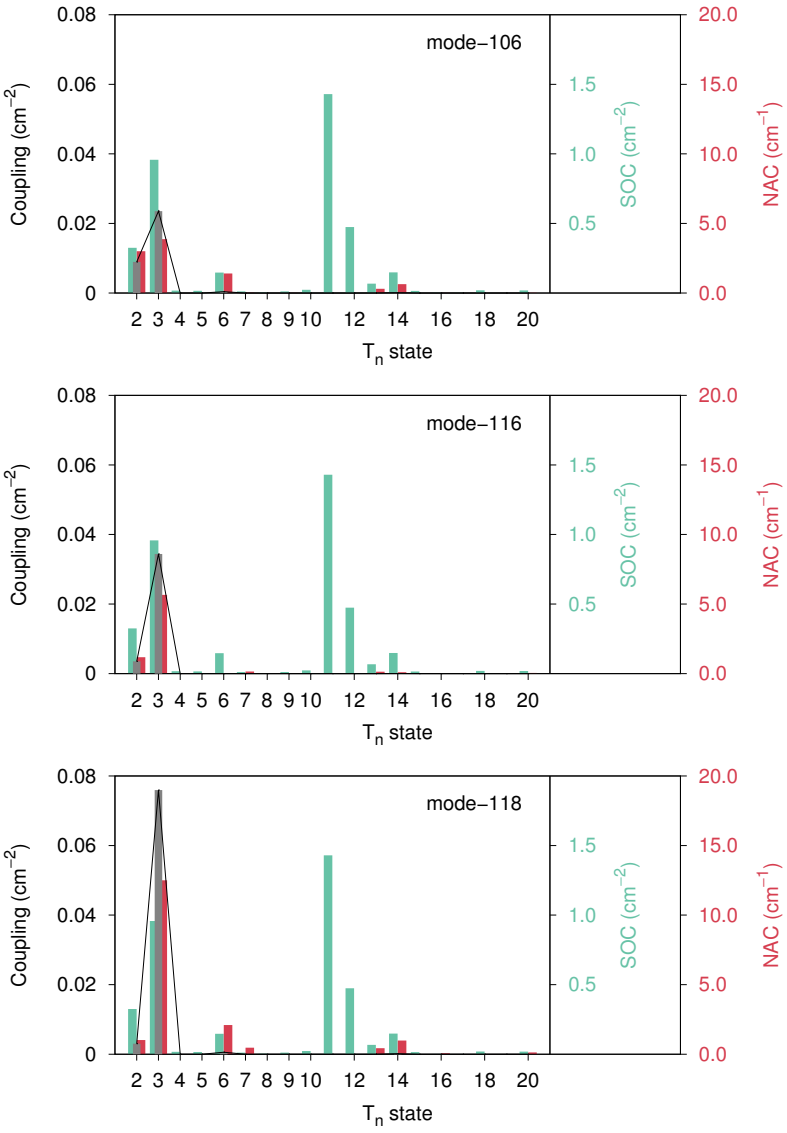

Figure S2: Spin–orbit (green) and mode-projected nonadiabatic (red) couplings contributed by each triplet state to the spin–vibronic term. Only the electronic terms are shown. Projections were carried out onto each mode vector, normalized in the atomic unit ($\sqrt{m_e}\cdot$bohr). The combined coupling including the energy denominator is also shown in gray.

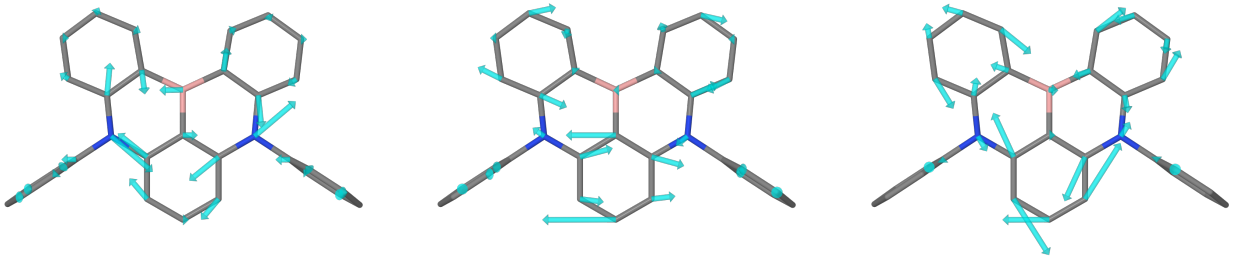

ν_{106} at 1279 cm^{-1} ν_{116} at 1402 cm^{-1} ν_{118} at 1426 cm^{-1}

Figure S3: Important normal vibrations of DABNA in the S_1 state. T_1 vibrational motions are very similar and cannot be visually distinguished from the S_1 ones. Hydrogen atoms are omitted for visual clarity.

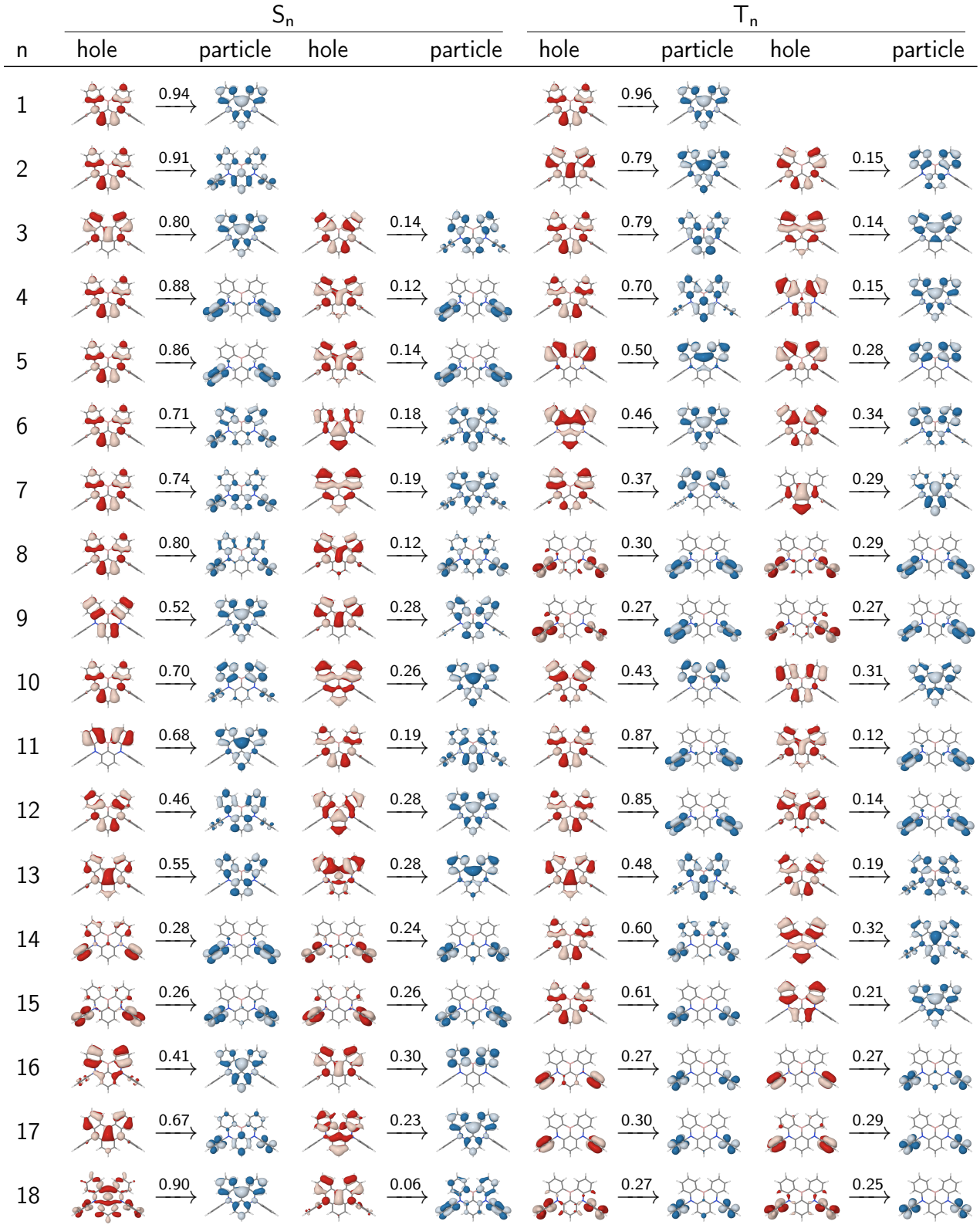

Figure S4: Natural transition orbital (NTO) pairs at the ω*B97X level with Tamm-Dancoff approximation for the excited states of DABNA. Hole (red) and particle (blue) wavefunctions with dominant weights are shown.

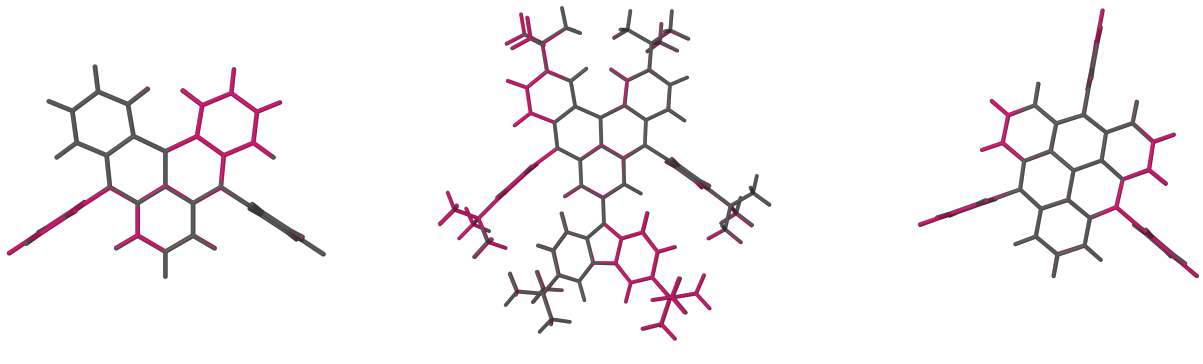

Figure S5: Exited state geometries of MR-TADF emitters. The S_1 and the T_1 geometries are respectively shown in gray and magenta. The geometries were aligned with the Eckart condition and the corresponding root-mean-squared deviations (in Å) are given in parentheses.

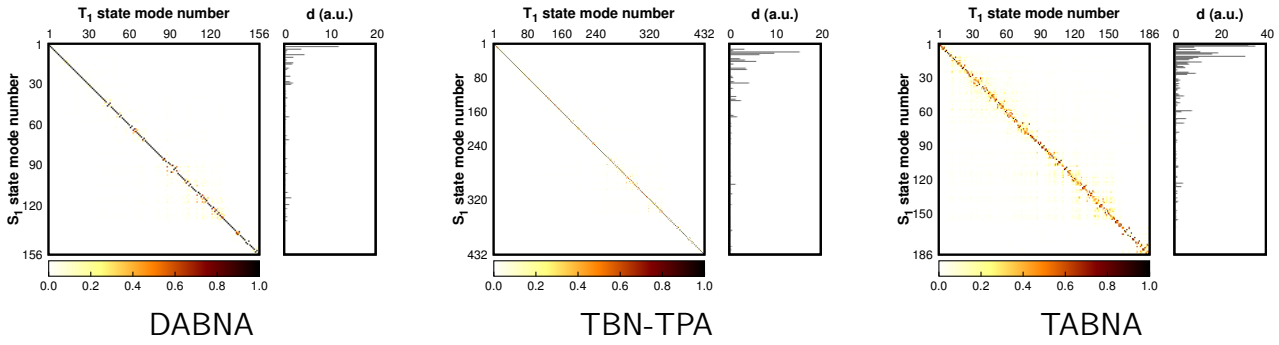

Figure S6: Duschinsky matrices and displacement vectors related to the RISC transitions. The sizes of the matrix and the vector elements are displayed with their absolute values.

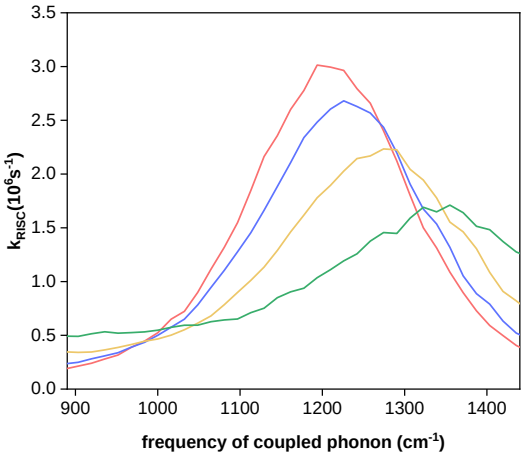

Figure S7: Effect of fictitiously increasing the emitter-specific S_1–T_1 reorganization energy λ'_{em} on the resonance enhancement of RISC rate, estimated with PBME-nH simulations. The red line displays the rate profile with the physical reorganization energy, $\lambda'_{\mathrm{em}} = \lambda_{\mathrm{em}}$, as obtained with the SCS-ADC(2)/SVP level. Blue, yellow, and green lines progressively show the profiles with $\lambda'_{\mathrm{em}} = 2\lambda_{\mathrm{em}}$, $4\lambda_{\mathrm{em}}$, and $8\lambda_{\mathrm{em}}$. Fictitiously increasing λ'_{em} is equivalent to increasing the S_1–T_1 geometric displacement $\vec{d}'$ as employed in Figure 6 in the main text. It is apparent that the resonance enhancement diminishes with a larger displacement, in agreement with Figure 6b.

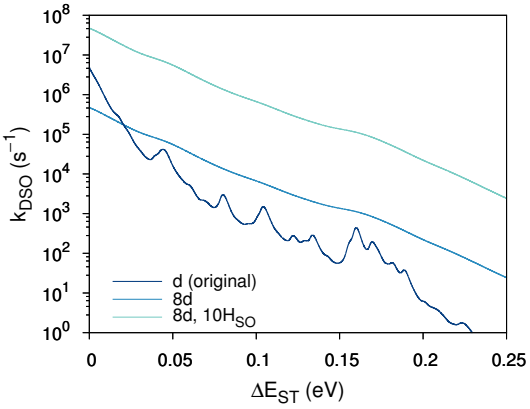

Figure S8: Displacement dependence of the first-order direct spin–orbit RISC rates at varying ΔE_{ST}. The original displacement vector $\vec{d}$ of DABNA was modified as in Figure 6b. At large $\vec{d}' = 8\vec{d}$ (corresponding to $\lambda = 2128$ cm^{-1}) with $H'_{\mathrm{SO}} = 10H_{\mathrm{SO}}$ (corresponding to 0.35 cm^{-1}), k_{DSO} behaves similarly to the rate in DA-TADF emitters (ref S1).

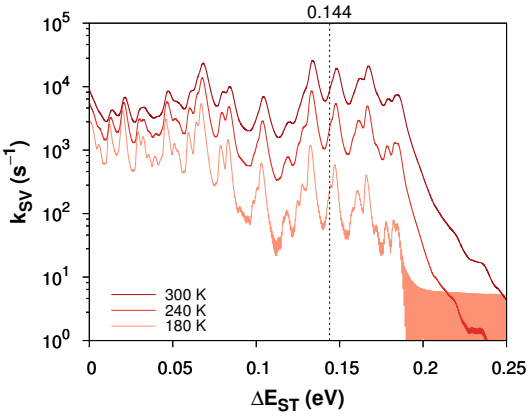

Figure S9: Temperature dependence of the RISC rates of DABNA. ΔE_{ST} value from the SCS-CC2 level is marked with a vertical line.

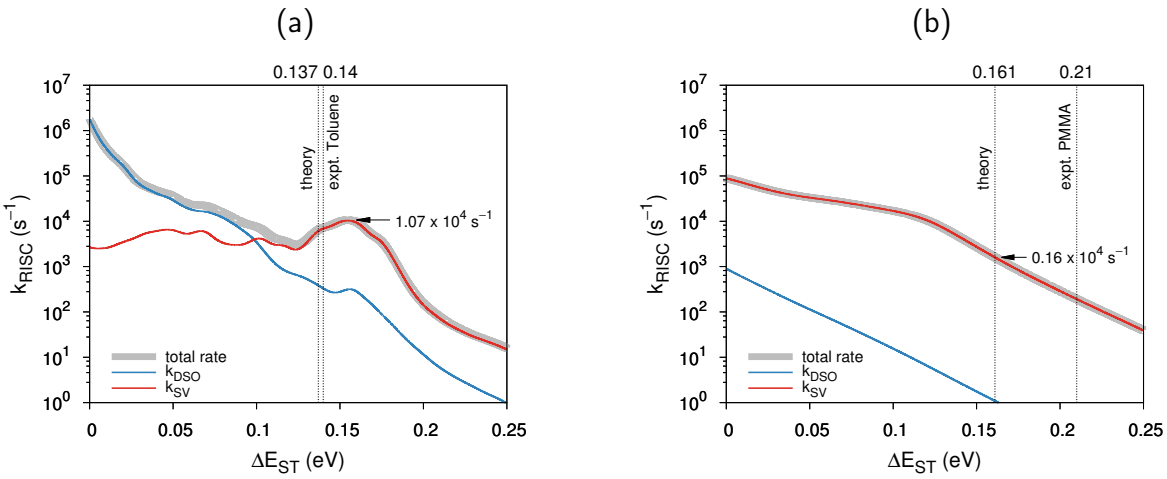

Figure S10: Total RISC rate and its decomposition into DSO and SV conbributions for MR-TADF emitters at varying ΔE_{ST} values: (a) TBN-TPA; (b) TABNA. ΔE_{ST} values from the SCS-CC2 level and experiments are marked with vertical lines.

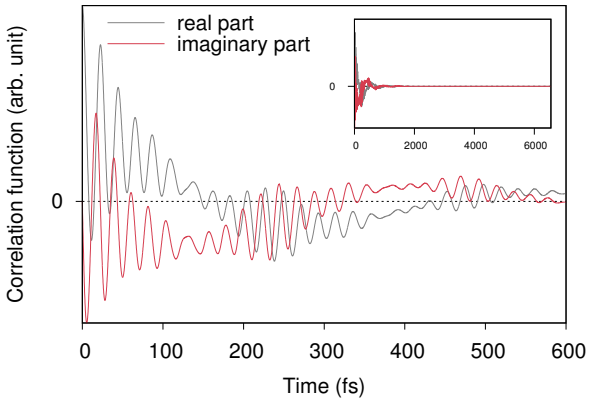

Figure S11: Time correlation function for DABNA in the positive time segment before the Fourier transform. The real part is even and the imaginary part is odd with respect to time inversion. Inset shows the same function to the integration limit of 6553.6 fs.

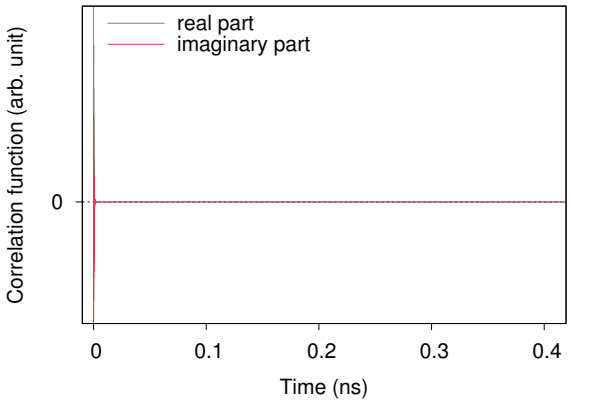

Figure S12: Long time behavior of the time correlation without any approximation for DABNA.

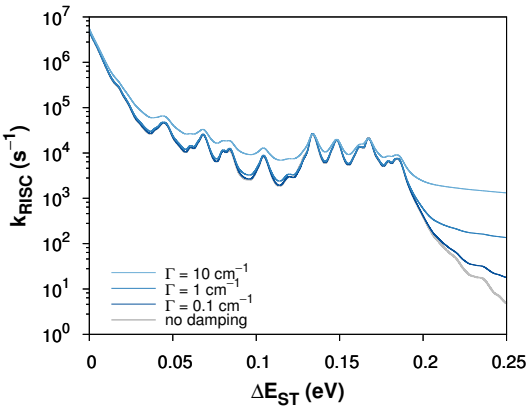

Figure S13: Effect of damping on k_{RISC}. Damping was implemented as a Lorentian function $\delta'(-\Delta E_{\mathrm{ST}} + E_v - E_{v'}) = \Gamma/\pi[\Gamma^2 + (\Delta E_{\mathrm{ST}} - E_v + E_{v'})^2]$ in the place of $\delta(-\Delta E_{\mathrm{ST}} + E_v - E_{v'})$ in eq S6.

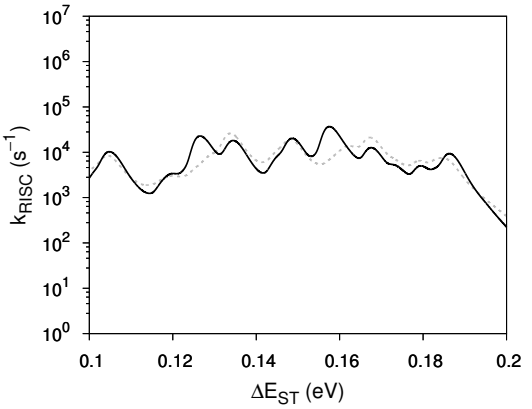

Figure S14: Rate change by approximating the Duschinsky rotation as $\mathbf{J} = \mathbf{1}$ for DABNA. The black solid line represents the rate after the approximation, while the gray dashed line shows the original data before the approximation as provided in Figure 2a in the main text.

Supporting Information References

[S1] Kim, I.; Jeon, S. O.; Jeong, D.; Choi, H.; Son, W. J.; Kim, D.; Rhee, Y. M.; Lee, H. S. *J. Chem. Theory Comput.* **2020**, *16*, 621–632.

[S2] Marian, C. M. *Wiley Interdiscip. Rev. Comput. Mol. Sci.* **2012**, *2*, 187–203.

[S3] May, V.; Kühn, O. *Charge and Energy Transfer Dynamics in Molecular Systems*, 3rd ed.; Wiley-VCH, 2011.

[S4] Ou, Q.; Bellchambers, G. D.; Furche, F.; Subotnik, J. E. *J. Chem. Phys.* **2015**, *142*, 064114.

[S5] Peng, Q.; Niu, Y.; Shi, Q.; Gao, X.; Shuai, Z. *J. Chem. Theory Comput.* **2013**, *9*, 1132–1143.

[S6] Baiardi, A.; Bloino, J.; Barone, V. *J. Chem. Theory Comput.* **2013**, *9*, 4097–4115.

[S7] De Souza, B.; Farias, G.; Neese, F.; Izsák, R. *J. Chem. Theory Comput.* **2019**, *15*, 1896–1904.

[S8] Reimers, J. R. *J. Chem. Phys.* **2001**, *115*, 9103–9109.

[S9] Friese, D. H.; Törk, L.; Hättig, C. *J. Chem. Phys.* **2014**, *141*, 194106.

[S10] Niu, Y.; Peng, Q.; Deng, C.; Gao, X.; Shuai, Z. *J. Phys. Chem. A* **2010**, *114*, 7817–7831.

[S11] Etinski, M.; Tatchen, J.; Marian, C. M. *J. Chem. Phys.* **2011**, *134*, 154105.

[S12] Kim, H. W.; Rhee, Y. M. *J. Chem. Phys.* **2014**, *140*, 184106.

[S13] Kim, C. W.; Park, J. W.; Rhee, Y. M. *J. Phys. Chem. Lett.* **2015**, *6*, 2875–2880.

[S14] Kim, H.; Nassimi, A.; Kapral, R. *J. Chem. Phys.* **2008**, *129*, 084102.

[S15] Bonella, S.; Coker, D. F. *J. Chem. Phys.* **2003**, *118*, 4370–4385.

[S16] Mandal, A.; Yamijala, S. S.; Huo, P. *J. Chem. Theory Comput.* **2018**, *14*, 1828–1840.

[S17] Zhou, W.; Mandal, A.; Huo, P. *J. Phys. Chem. Lett.* **2019**, *10*, 7062–7070.

[S18] Park, J. W.; Rhee, Y. M. *J. Chem. Phys.* **2014**, *140*, 164112.

[S19] Park, S. W.; Yang, J. H.; Choi, H.; Rhee, Y. M.; Kim, D. *J. Phys. Chem. A* **2020**, *124*, 10384–10392.